Nanoparticle-Enhanced Near Infrared Fluorescence Imaging of Atheroma Detects Thrombosis-Prone Plaques Prior to Rupture

TABLE OF CONTENTS

ABSTRACT

Introduction: Acute coronary syndromes - including unstable angina, acute myocardial infarction and sudden death - are primarily due to sudden luminal thrombosis from disruption of an atherosclerotic plaque. It has been established that inflammation plays an important role in atherogenesis and the destabilization of plaques. However, the role of inflammation in catalyzing plaque rupture is incompletely understood. Here, we experimentally investigated the *in vivo* spatial distribution of a novel atheroma cell targeted near-infrared fluorescence (NIRF) imaging agent, CLIO-CyAm7, prior to triggered plaque rupture, using intravascular molecular imaging. We hypothesized that CLIO-CyAm7 would illuminate macrophages on *in vivo* intravascular NIRF imaging and preferentially localize to atheroma that develop plaque thrombosis under triggering conditions.

Methods: Atherosclerosis was induced in rabbits (n=28) using a 12-week hyperlipidemic diet with alternating 1% high cholesterol and normal chow with concomitant aortic balloon injury at 2 weeks. Rabbits were injected with 2.5mg/kg of CLIO-CyAm7 24 hours prior to *in vivo* imaging. *In vivo* NIRF and intravascular ultrasound (IVUS) imaging were used to assess baseline structural and inflammation characteristics of atheroma. Control rabbits (n=6) were sacrificed prior to triggering. Pharmacological triggering was performed using Russell's Viper Venom (0.15mg/kg IP) and histamine (0.02mg/kg IV) injections twice over 48-hours. IVUS imaging was repeated prior to sacrifice to identify luminal thrombi *in vivo*. NIRF imaging was quantified using target-to-background ratio (TBR), the ratio between an area of atheroma compared to normal, uninjured aorta. A subset of rabbits (n=7) was injected with Evans Blue (6mL 0.5% IV) 30 minutes prior to sacrifice to identify permeability of the endothelium. After sacrifice, *ex vivo* imaging, fluorescence microscopy (FM), RAM-11 immunofluorescence (IF) of macrophages, alpha-smooth muscle actin IF for smooth muscle cells, CD31 IF for endothelial cells, and Carstairs' staining for fibrin and collagen, were performed systematically along the length of the aorta at 1.5cm increments. Data is presented as mean±SD.

Results: On microscopy, CLIO-CyAm7 localized primarily at the intimal-luminal border of atheroma, with some penetration into the media and adventitia. There was significantly higher CLIO-CyAm7 accumulation in areas of atheroma compared to control segments of the aorta (1.73±1.9% vs. 0.13±0.28%, $p<0.0001$). On IF, CLIO-CyAm7 signal correlated with subsets of macrophages, endothelial cells and smooth muscle cells in atheroma with minimal CLIO-CyAm7 evident in normal arteries. Evans blue showed increased endothelial permeability in regions of increased subendothelial CLIO-CyAm7 accumulation. CD31+ endothelial cells in the neovessels at the intima-media border indicated delivery of CLIO-CyAm7 via vaso vasorum. *In vivo,* CLIO-CyAm7+ plaques were detectable via intravascular NIRF imaging. Areas of atherosclerosis, determined by IVUS, showed significantly higher NIRF peak TBR than normal segments of the aorta (2.86±1.82 vs. 1.55±0.65, $p=0.001$). *In vivo* IVUS imaging and Carstairs' staining for fibrin identified plaque thrombosis in 10 of 15 rabbits undergoing the triggered protocol (67%). Notably, plaques with luminal thrombosis showed significantly higher CLIO-CyAm7 accumulation compared to undisrupted atheroma (2.1±1.7% vs. 1.5±1.9%, $p=0.0446$), indicating that atheroma cell phagocytic capacity may underlie plaque rupture.

Conclusion: CLIO-CyAm7 is a novel NIRF molecular imaging agent that identifies a subset of phagocytically active cells that are increased in atheroma prone to plaque thrombosis. Intravascular 2D NIRF imaging provides a promising future translational tool for high-resolution imaging of biologically high-risk plaques.

GLOSSARY

ACS: acute coronary syndrome
aSMA: α-Smooth muscle actin
CAC: coronary artery calcification
CAD: coronary artery disease
CLIO: cross-linked iron oxide
CT: computed tomography
CTA: CT-angiography
CVD: Cardiovascular disease
^{18}F-NaF: [^{18}F]fluoro-sodium fluoride
^{18}FDG: 2-Deoxy-2-[^{18}F]fluoro-D-glucose
FM: fluorescence microscopy
FRI: fluorescence reflectance imaging
HCD: high cholesterol diet
IF: immunofluorescence
IVUS: intravascular ultrasound
LDL: low density lipoprotein
MI: Myocardial infarction
MION: monocrystalline iron oxide
MMP: matrixmetalloproteinase
NIRF: near-infrared fluorescence
OCT: optical coherence tomography
OFDI: optical frequency domain imaging
PCCT: phase-contrast CT
PET: positron emission tomography
ROI: region of interest
RVV: Russell's viper venom
SMC: smooth muscle cell
SNR: signal-to-noise ratio
TBR: target-to-background
TCFA: thin cap fibroatheroma
SPIO: superparamagnetic ironoxide
USPIO: ultrasmall superparamagnetic iron oxide

INTRODUCTION

Atherosclerosis is a systemic inflammatory disease leading to expansion of the innermost layer of the artery, the intima, which may lead to coronary artery disease (CAD), stroke, and peripheral arterial disease. Although atherosclerosis is progressive and may cause gradual stenosis of the arteries, the most devastating effects of this disease occur due to the development of sudden occlusive thrombi and subsequent end-organ ischemia and infarction. In the coronary arteries specifically, the results of thrombus formation may include acute myocardial infarction (MI), unstable angina and sudden death, collectively called acute coronary syndrome (ACS). The majority of these patients are often asymptomatic because earlier stages of CAD, like stable angina, may not limit blood flow to the myocardium.

The ability to precisely identify patients who will develop symptomatic atherosclerotic syndrome is currently unavailable. Traditional risk factors, like family history, cholesterol, tobacco use and diabetes mellitus, can be used to categorize patients into levels of risk, however, this information cannot assess the temporal or localized risk of ACS or responsiveness to therapy. The majority of ACS events result from lesions with less than 50% stenosis. However, current methods of imaging, such as x-ray angiography, focus on anatomical changes like vessel narrowing and miss these culprit lesions prior to an acute event. (1) This leads to the importance of new diagnostic imaging in the assessment of high-risk patients.

Atherosclerosis is a complex biological process that is not fully characterized by current imaging tools.(2-4) New molecular imaging techniques that focus on basic biological processes, like inflammation, may provide the necessary information to identify the lesions in patients at highest immediate risk of thrombosis.(5-8) In this study, we used a novel magneto-optical imaging agent, CLIO-CyAm7 with an *in vivo* intravascular near infrared fluorescence (NIRF) imaging system to assess levels of inflammation prior to triggered plaque rupture in a rabbit model of atherothrombosis. We hypothesized that more inflamed plaques are increasingly susceptible to plaque disruption and thrombus formation.(2)

Clinical Importance of Coronary Artery Disease

Cardiovascular disease (CVD) is the leading cause of death world wide, and as the rates of obesity and diabetes are increasing, the burden of CVD is expected to grow.(9) Although the mortality from coronary artery disease has been decreasing over the past decades, this change is largely a result of improved medical and surgical treatment of this condition. The cost of

managing this disease is only increasing. In 2009, CAD cost $195.2 billion and this cost is projected to double by the year 2030.(9) Therefore, it is imperative to improve methods of detection for individuals at risk for ACS to prevent the significant morbidity and mortality related to these conditions.

Mechanisms of Atherosclerosis and Human Vulnerable Plaque Rupture

Evolution of Atherosclerotic Plaques

The biological process behind the development of atherosclerosis involves an evolution of atherosclerotic plaque from harmless "fatty streaks" to complex plaques that are vulnerable to plaque rupture. During the initial stages of atherosclerosis, low density lipoproteins (LDL) from the bloodstream accumulate in the vessel wall below the endothelium. Endothelial cells are then activated due to the accumulation and oxidation of LDL, leading to the expression of adhesion molecules and release of cytokines that recruit monocytes and enhance their migration into the subendothelium.(10, 11) In this inflammatory state, endothelial dysfunction leads to increased permeability and an impaired ability to protect the underlying vessel wall. Specific patterns of blood flow, like low shear stress, also activate the endothelium, increasing the frequency of atheroma in areas of disturbed flow, like bifurcations. Within these early plaques, monocytes differentiate into macrophages and continue to accumulate intracellular lipids, becoming foam cells. These asymptomatic "fatty streaks" can be seen as early as adolescence or young adulthood.(12)

Over time, the inflammatory process continues to promote macrophage accumulation with increasing T-cell and smooth muscle cell (SMC) infiltration. Fibroblast-like SMCs produce collagen, creating a fibrous cap covering the luminal surface of the atherosclerotic lesion. The role of SMCs in the atherosclerotic plaque is complex. It is thought that within atheroma, SMCs switch phenotypes from the typical contractile phenotype found in the media to a synthetic phenotype capable of more efficiently producing extracellular matrix components, including collagen and elastin, which are required to develop a fibrous cap to prevent plaque rupture.(13) In fact, many SMCs in the intima may not express the typical cell markers, including α-Smooth muscle actin, and even transdifferentiate into macrophage-like cells and accumulate cholesterol.(14, 15) Interestingly, evidence is building that there is a third "proinflammatory" SMC phenotype within atheroma, where SMCs produce cell adhesion molecules and cytokines to promote macrophage migration and atherosclerosis development.(15-17) In this way, SMCs play conflicting roles to both promote the growth of atheroma by sustaining the inflammatory

state and stabilize these plaques by producing collagen and fibrosis to prevent plaque rupture.

Beneath the fibrous cap, a necrotic core may form due to apoptosis of plaque macrophages. Prolonged endoplasmic reticulum stress and ineffective clearance of these cells from the plaque induce apoptosis.(18) Endoplasmic reticulum stress can be increased by insulin resistance, leading to larger necrotic cores in patients with type 2 diabetes. Calcification also occurs within the lesions as a result of SMC death.

The hypoxic necrotic core leads to the secretion of angiogenic factors, causing neovascularization. Neovessels generally originate from the adventitial vaso vasorum and penetrate through the media into the intimal base. These new, fragile blood vessels have an increased permeability and are prone to rupture, causing intraplaque hemorrhage.(13)

Mechanism of Plaque Rupture

ACS is a result of sudden luminal thrombosis and is primarily caused by either plaque rupture or erosion. Plaque ruptures most commonly occur in lesions categorized as thin cap fibroatheroma (TCFA). The major features of a TCFA are a thin fibrous cap <65um with decreased SMCs overlying a necrotic core. When this fibrous cap is disrupted, the thrombogenic necrotic core is exposed to luminal blood, fostering thrombus formation. In a study of human plaques at autopsy, ruptured plaques similar to TCFA had larger necrotic cores, increased macrophages in the fibrous cap, and greater calcification.(19) In plaque erosion, loss of endothelium causes an interaction between both the SMC and proteoglycan rich intima and luminal blood, leading to thrombus formation.

Role of Macrophages in Plaque Progression

Macrophages play a major role in the development of TFCA that are vulnerable to plaque rupture. To develop a thin fibrous cap, two major processes can occur: decreased production of fibrous tissue and/or increased destruction of existing fibrous tissue. The fibrous cap is made primarily of collagen produced by migrating SMCs. Plaque macrophages can trigger SMC apoptosis by activating the Fas ligand apoptotic pathway directly, and by releasing extrinsic factors that trigger apoptosis, like nitric oxide and TNF-alpha.(20) Additionally, inflammatory macrophages decrease the production of collagen in SMCs. As part of their normal maintenance function, macrophages produce matrixmetalloproteinases (MMPs) and cystein proteases that break down collagenous and elastin components of extracellular matrix. In the highly inflammatory environment of a plaque, there is an increased production of MMPs by

macrophages, leading to a thinning of the fibrous cap via breakdown of collagen. As the fibrous cap progressively thins, the plaque is increasingly vulnerable to rupture.

Current Methods of Coronary Artery Atherosclerosis Structural Imaging

Due to the high societal burden of this disease, a variety of imaging tools are currently clinically used to assess atherosclerosis. Starting with traditional angiography to map stenosis in the vessel lumen, a wide variety of other invasive and non-invasive imaging modalities have been used to detect vulnerable plaques based on specific characteristics described previously, including a thin fibrous cap, inflammation, lipid core, and calcification. These developments have provided new insights into the progression of atherosclerosis and enhanced the ability to diagnose and follow treatment of systemic atherosclerosis.

Non invasive Coronary Artery Imaging

Non-invasive structural coronary artery imaging primarily utilizes computed tomography (CT) imaging due to its high temporal and spatial resolution, although MRI has also realized some success in coronary imaging due to the high spatial resolution and better soft tissue contrast. All noninvasive imaging modalities are limited by the small size of the coronary artery lumen and significant motion artifacts due to both respiration and cardiac motion.

CT imaging measures atherosclerosis either using non-contrast imaging to quantify coronary artery calcification (CAC) or using CT-angiography (CTA) to detect vessel stenosis. CAC scoring quantifies calcification in the coronary arteries. In complex lesions, necrotic SMCs become calcified and are detectable by x-ray based imaging as radiopaque inclusions in the vessel wall. Specifically, the MESA study showed a 7-10x increased risk of CAD in patients with a CAC score >100.(21) CAC scoring clinically improves prediction of a patient's overall risk of a cardiovascular event by assessing the overall disease burden, rather than identifying individual lesions that may lead to such an event. A major disadvantage of CAC as a marker of plaque calcification is the inability to detect microcalcifications, which play a major role in the mechanical destabilization of plaques.

High resolution CTA determines the extent of stenotic CAD by visualization of the lumen of the coronary arteries using an injected iodinated contrast agent, similar to a conventional x-ray angiogram. This is effective in identifying obstructive and non-obstructive CAD, particularly in intermediate risk patients with symptoms. In high-risk patients, invasive angiography is preferred due to the ability to provide immediate intervention. The major disadvantages to CT imaging of

the coronary arteries are the dose of ionizing radiation and nephrotoxicity of contrast agents, which are often used in higher doses than conventional angiography. Although the radiation dose has been steadily minimized with improved imaging techniques and scanners, this remains a problem if the technique is to be used as an ongoing screening tool. Additionally, in patients with highly calcified vessels, the calcification may interfere with interpretation of the contrast agent.

Current CT imaging is limited by the low soft tissue contrast due to the small differences in x-ray attenuation between these tissues. A newer technique, phase-contrast CT (PCCT) differentiates between tissues based on the x-ray phase shift as the wave passes through different tissues. This technique improves the soft tissue contrast compared to standard attenuation based CT while still maintaining the high spatial resolution of conventional CT. *Ex vivo* studies of human carotid arteries and ApoE (-/-) mouse aortas showed the potential of PCCT to identify a fibrous cap, necrotic core, intraplaque hemorrhage and calcification. (22-24) PCCT has steadily moved closer to clinical use with the development of techniques using a standard x-ray source and a grating interferometer.

There has been promising work using the natively high soft tissue contrast of MRI to further characterize atherosclerotic plaques noninvasively. Earlier work with MRI of the arterial wall focused on imaging of the carotid artery and the aorta due to the larger lumen diameters and decreased motion artifact. In the carotid artery, noncontrast MRI was able to determine wall thickness, presence of a necrotic core, fibrous cap and plaque hemorrhage.(25, 26) In particular, measurement of plaque hemorrhage is well suited to MRI. The hypoxic environment of the necrotic core leads to conversion of hemoglobin to methemoglobin, which has inherent paramagnetic properties that shorten the T1 relaxation and produce a hyperintense signal on T1 imaging.(27) Unenhanced MRI has been used in human coronary arteries to identify the vessel wall thickness, evidence of positive remodeling, and plaque hemorrhage.(25, 28-32) MRI also has potential to investigate pathologic function of the vessels. For example, one study identified impaired endothelial-induced vasodilation during physical exercise in patients with CAD compared to healthy controls. Additionally, in patients with CAD vasodilation was significantly higher in vessels with minimal atherosclerotic plaques compared to vessels with significant disease burden.(33)

Furthermore, gadolinium enhanced MRI has been used to further characterize atherosclerotic plaques in both the carotid and coronary arteries. Gadolinium is transported intravascularly, therefore, it is preferentially delivered to plaques with increased neovascularization. The

necrotic core has decreased blood flow and does not enhance with contrast administration. Delayed-enhancement imaging detects contrast that has extravasated from the vasculature and signifies decreased clearance, often due to fibrosis. Delayed enhancement of the coronary artery wall has been correlated with severity of atherosclerosis confirmed by CT and X-ray angiography.(25, 34)

Invasive Coronary Artery Structural Imaging

Intravascular imaging, while invasive, offers close proximity to the target tissue and minimal motion artifacts, key factors for obtaining high quality images of coronary atheroma. Current clinical intravascular imaging techniques include traditional x-ray angiography, intravascular ultrasound (IVUS) and newer optical based structural imaging tools like optical coherence tomography (OCT) and optical frequency domain imaging (OFDI).

X-ray angiography is the gold standard clinical tool to assess CAD. However, this imaging technique underestimates the true extent of plaque progression, especially early in the disease. Earlier in the progression of atherosclerosis, there is a tendency towards positive remodeling, the growth of plaque into the wall of the vessel rather than into the lumen. These changes are not visible when only imaging the luminal contour of the artery. Angiography is most useful in detection of critical stenoses and luminal thrombi as a prelude to coronary revascularization.

IVUS has gained widespread clinical acceptance for assessment of coronary atherosclerosis. IVUS imaging uses ultrasound waves emitted from a transducer at the end of a catheter to provide structural characteristics of atheroma, such as plaque volume, eccentricity, and positive or negative remodeling. In patients with CAD, IVUS demonstrates widespread atheroma well beyond that identified with angiography.(1) Specifically, studies using IVUS have found that plaque rupture is more common in lesions with positive remodeling and a higher plaque burden. IVUS is limited in its ability to visualize the thin fibrous cap due to its relatively low resolution (0.08-0.1mm).(35)

IVUS allows further analysis beyond traditional amplitude visualization, including radiofrequency component analysis from the backscatter signal. Each component of a plaque has different signature backscatter properties based on the molecular makeup of their constituents.(36) To utilize this information, Virtual Histology (VH-IVUS) is based on an autoregressive spectral analysis of radiofrequency backscatter. The system outputs a color image that distinguishes between fibrous, fibrofatty, necrotic core, and calcified tissue. The PROSPECT study, the first study to perform serial IVUS imaging of non-culprit lesions, demonstrated that morphological

assessment of plaques by IVUS can predict the occurrence of coronary events.(1) However, the limited accuracy determined in this trial precludes routine clinical usage of VH-IVUS.(37)

OCT is similar in concept to IVUS imaging, but utilizes an infrared light source instead of ultrasonographic waves. Compared to IVUS, OCT has a 10-fold higher resolution (10um), allowing visualization of thin fibrous caps (<65um), necrotic cores, and inflammatory cells.(24, 35) Recently the high resolution of OCT was harnessed in the EASY-FIT study, a randomized control trial of high- and low-dose atorvastatin, to determine the effect of statins on the thickness of the fibrous cap. The study showed that over a one-year period, a higher dose of atorvastatin correlated with a significantly increased fibrous cap thickness.(38) The major disadvantage of OCT is the inability to image through blood and limited depth penetration, necessitating flushing with saline to obtain images of the vessel wall or within larger coronary arteries. The limited depth of imaging, 1-2mm even in the presence of saline, hinders the measurements of plaque burden or remodeling index, which are generally obtained using IVUS. Second generation OCT, optical frequency domain imaging (OFDI), has a faster acquisition time and a larger field of view, allowing imaging without the need to occlude the target vessel.(39) OFDI and OCT are now being combined with optical near-infrared fluorescence imaging systems to provide both structural and biological assessments.(40)

Molecular Imaging of Atherosclerosis

The above-mentioned imaging modalities focus on the structural characteristics of atheroma, however, many targeted imaging approaches are being developed to specifically image the biological changes that lead to vulnerable plaques. Multiple processes leading to plaque rupture are currently being investigated, including inflammation, necrosis, neovascularization, thrombosis, and microcalcification.(5-8, 41) Because inflammation is widely considered to play a vital role in the development of vulnerable plaques, it is an active area of research with imaging agents addressing a wide variety of inflammatory processes.(11, 42)

Positron Emission Tomography

Positron emission tomography (PET) imaging has emerged as a method for detecting the role of inflammation non-invasively in atherosclerosis. PET imaging is a nuclear imaging technique that relies on a radioactive tracer that decays, emitting detectable positrons. PET has a high sensitivity because it can detect a very small quantity of tracer, but it has very limited spatial resolution. 2-Deoxy-2-[^{18}F]fluoro-D-glucose (^{18}FDG) is commonly used in cancer imaging as a marker for areas with high metabolic activity. In atherosclerosis, the relatively avascular plaque

creates an anaerobic microenvironment, increasing the glucose metabolism of inflammatory cells. Therefore, ^{18}FDG-PET is a sensitive marker of vascular atherosclerosis. Specifically, multiple studies have indicated that the major source of this signal is from macrophages.(35, 43) In particular, ^{18}FDG-PET is taken up preferentially by proatherogenic, M1 macrophages compared to M2 macrophages.(44) Additionally, plaque hypoxia has been found to correlate with an increase in ^{18}FDG-PET signal.(45) However, the low resolution of PET imaging (4mm), difficulty with cardiac gating, and the high background signal of the myocardium limit the use of this modality to the carotid arteries and aorta in humans, with just a few examples in human coronary arteries.(35)

To reduce the background signal from the myocardium, various more targeted PET tracers have been developed, generally an adaptation of cancer imaging agents. For example, the somatostatin receptor, which is upregulated in multiple diseases including neuroendocrine tumors, was found to be upregulated in inflammatory macrophages and activated endothelium in atherosclerosis. Therefore, a somatostatin receptor targeted tracer, ^{68}Ga-DOTATATE, was looked at retrospectively in a cohort of patients receiving the tracer for cancer diagnosis. They found that the tracer uptake correlated with calcified plaques and previous cardiovascular events. This has been verified in animal models and is currently being studied clinically in the VISION study.(46) Recently, ^{18}F-Sodium fluoride (^{18}F-NaF) was compared to ^{18}FDG-PET in a prospective clinical trial of patients with myocardial infarction and stable angina. ^{18}F-NaF is thought to incorporate with hydroxyapatite within plaque calcifications and microcalcifications. In patients with MI, ^{18}F-NaF showed higher uptake in the culprit lesion, while ^{18}FDG-PET showed no increase in signal - largely due to the high background signal. Additionally, in patients with stable angina, ^{18}F-NaF uptake correlated with high-risk features on IVUS.(47)

Magnetic Resonance Imaging

Magnetic resonance imaging (MRI) is used for molecular imaging of atherosclerosis due to its high spatial resolution, good soft tissue contrast and the existence of two major contrast agents that can be conjugated to multiple imaging targets: gadolinium and iron oxide.(25)

Gadolinium is a T1 shortening agent that has been conjugated to multiple targets, including albumin, fibrin and elastin. A gadolinium based albumin-binding agent, gadofosveset, has been used in an apoE(-/-) mouse model to detect endothelial dysfunction based on permeability of the vessel wall.(48) A fibrin target agent, EP-2104R, has been shown to detect thrombi in vivo in a phase II clinical trial.(49, 50) Elastin is initially broken down by proteases as a result of

inflammation in the atherosclerotic plaque, however, over time there is a response of overproduction of elastin. Therefore, elastin has been investigated as a sign of vascular remodeling, particularly in the context of stent placement.(51)

Iron oxide molecules are the second major category of MRI contrast agents, which exert a strong T2 shortening effect. Iron oxide is divided into superparamagnetic iron oxide (SPIO) and ultrasmall superparamagnetic iron oxide (USPIO) particles. SPIOs have a shorter blood half-life (~5 minutes) and are primarily used clinically for imaging the liver. USPIOs, which have a longer half-life (~10-24 hours), have now been used for molecular imaging of atherosclerosis, myocardial infarction and cancer.(25) These agents can be directly detected using MRI because the superparamagnetic nature creates a disturbance of the magnetic field that can be visualized as a decreased signal on a T_2^*- weighted image. USPIOs can be differentiated based on the composition of the iron oxide core or the surface coating. The hydrophilic surface coating on USPIOs is necessary to stabilize the particle and prevent aggregation.(52)

USPIOs have been used in a wide variety of clinical applications. Ferumoxtran-10, a USPIO with a dextran coating, has been used in human research studies to study atherosclerosis in the aorta, pelvic arteries and carotid artery.(52) Additionally, ferumoxytol, an FDA approved USPIO for treatment of iron deficiency anemia in the context of chronic kidney disease, has been used clinically to detect acute MI. However, it is unclear if there is sufficient sensitivity to detect atherosclerosis in the coronary arteries using this method. In the ATHEROMA study, USPIOs were used to assess the effects of high-dose vs. low-dose atorvastatin on macrophage activity in human carotid arteries by detecting a decrease in USPIO-induced signal loss.(53) Similarly, in a rabbit model of atherosclerosis, monocrystalline iron oxide nanoparticles (MIONs) were used to visualize atheroma in a study determining the effect of treatment with rosuvastatin. This study showed that MIONs colocalized with macrophages and *in vivo* imaging could show a decrease in macrophages in animals treated with statins.(54)

Another important subset of USPIOs, called cross-linked iron oxide (CLIO), are synthesized by cross linking the outer dextran surface coat of MIONs.(55) CLIO can be conjugated to improve the specificity of the particle and to develop multimodal imaging particles, e.g. magneto-optical nanoparticles. For example, VCAM-1 is an adhesion molecule that is expressed on the surface of endothelial cells in an inflammatory state, like atherosclerosis. A VCAM-1 targeted CLIO-fluorescence agent has been used to identify sites of atherosclerosis in the ApoE-/- mouse model.(56) Additionally, CLIO particles have been conjugated to both a fluorochrome for optical imaging and a nuclear imaging agent to allow multimodal imaging with MRI, PET and optical

imaging techniques.(57-59)

Protease Imaging

Another destabilizing factor in inflamed atherosclerotic plaques is the presence of MMPs, also a target for molecular imaging. One method of specifically imaging proteases is tagging nuclear imaging probes to small molecule protease inhibitors that can bind to the active site of the protease.(60) A second approach is the use of optical imaging agents that are activated by protease cleavage.(61-63) These protease sensors are an inert, non-immunogenic polylysine backbone with MPEG chains covalently linked and conjugated to a near infrared fluorescence dye. The polylysine backbone can then be cleaved by serine proteases to release the fluorescence agent. Due to the close proximity of the fluorophores on the polylysine backbone, these agents are autoquenched in their inactive form and are only visible on exposure to proteases. Therefore, the circulating form of the agent is inactive, lowering the background signal. This has been imaged by an intravascular near infrared fluorescence system through blood, eliminating the problems of cardiac motion and resolution.(63)

Despite these advances in molecular imaging of atherosclerosis, much is still unknown about the progression of atherosclerosis and how to predict the course of this disease. Therefore, new higher-resolution strategies to specifically target biological processes are being approached. Importantly, due to the complex nature of atherosclerosis, it will likely be necessarily to combine multiple imaging tools to create a truly predictive strategy for the diagnosis and management of high-risk vulnerable plaques.

Animal Models of Atherosclerosis and Thrombosis

Animal models of atherosclerosis and plaque rupture are essential for studying the mechanisms, treatment and diagnosis of vulnerable plaque rupture. Analogous to human vulnerable plaques, animal vulnerable plaques are defined as having a necrotic core, thin fibrous cap, and high inflammatory content. The most commonly used animal model of atherosclerosis is the ApoE -/- mouse model. On a high cholesterol diet, ApoE-/- mice develop atherosclerosis with spontaneous plaque rupture, especially in the brachiocephalic arch. However, detection of plaque rupture often depends on identification of buried caps, thought to be healed, non-occlusive plaque ruptures.(64) Additionally, this model does not produce coronary plaques. The mouse model is useful due to the ease of genetic manipulations to test mechanisms in atherosclerosis. However, the size of the mouse limits the use for clinical imaging investigations, especially intravascular, coronary artery-relevant approaches.

The most commonly used large animal model of atherosclerosis is the rabbit, as the rabbit aorta and iliac arteries are similar in caliber to the human coronary artery and recapitulate many aspects of human atheroma. This is especially useful in the study of clinical imaging systems, including intravascular imaging. Generation of atherosclerosis in the New Zealand white rabbit requires prolonged high cholesterol diet (HCD) along with endothelial denudation by aortic balloon injury. Additionally, there is a transgenic rabbit, called the Watanabe-heritable hyperlipidemic rabbit, that has a mutation causing an LDL receptors deficiency similar to familial hypercholesterolemia.(64, 65) These rabbits spontaneously produce atherosclerosis on a normal diet. After development of atherosclerosis in either model, plaque rupture has been induced using pharmacological triggering, direct perturbation of the endothelium using a balloon catheter, and electrochemical injury.(66-68)

The Constantinides rabbit model of atherothrombosis was created over 50 years ago to produce plaque disruption as a result of pharmacological triggering using Russell's Viper Venom (RVV), a procoagulant and endotoxin, and histamine, a vasoconstrictor.(69) Recently, this animal model has been optimized and has gained traction as a method for imaging vulnerable plaque rupture.(70) Histological analysis of this model has shown that ruptured plaques contained inflamed, thin fibrous caps, cholesterol crystals, and both medial and adventitial changes consistent with human vulnerable plaques. Additionally, inflammation, cholesterol content, and positive remodeling were found to be predictors of plaque rupture in this model.(70)

Multiple *in vivo* studies have been performed using the Constantinides model to determine risk factors for plaque rupture. It has been found that the structural characteristics, as determined by MRI, that increase susceptibility to plaque rupture are similar to those found in the PROSPECT trial, including larger plaque area, vessel area, remodeling ratio, and positive remodeling.(71) Additionally, MRI imaging has identified that regions of low endothelial shear stress are associated with these high risk characteristics and increased vulnerability to plaque rupture.(72) CT imaging has been shown to be unreliable in differentiating between tissues of varying composition, specifically between fibrous or lipid rich plaques.(73) Aziz et. al. used ^{18}FDG-PET with this rabbit model of atherothrombosis to assess the role of inflammation in plaque rupture. They found increased SUV_{max} in areas of plaques with rupture. However, due to the low resolution of PET imaging the ^{18}FDG signal analyzed covers a third of the aorta, potentially including multiple individual plaques. This study also showed a significantly higher macrophage density in plaques with thrombus, supporting the role of macrophages in plaque rupture.*(74)*

Near-Infrared Fluorescence Molecular Imaging of Atherothrombosis

In this study, a novel near-infrared fluorescence (NIRF) cellular imaging agent, CLIO-CyAm7, was used to detect inflammation using a catheter based intravascular NIRF imaging system. This agent consists of a cross-linked dextran coated monocrystalline iron oxide core conjugated to a fluorophore in the near-infrared light spectrum (650-1000nm). USPIOs and CLIO typically target inflammatory macrophages, but can also localize to abnormal endothelial cells and SMCs in atherosclerosis disease models.(57, 59) Both water and hemoglobin minimally absorb light at this wavelength, allowing NIR light to pass through blood and tissue efficiently, increasing the depth of signal penetration. Intravascular NIRF imaging has been developed by the Jaffer laboratory as a clinically translatable imaging tool for investigating human coronary arteries.(40, 62, 63) Intravascular imaging, as discussed previously, is ideal for the coronary arteries because it has gained widespread clinical acceptance for providing high-resolution coronary imaging, whereas noninvasive strategies are susceptible to large motion artifacts and insufficient spatiotemporal resolution. NIRF imaging is particularly translatable to clinical use because efficient light penetration allows imaging through blood.

Imaging of CLIO-CyAm7 with the intravascular NIRF imaging system allows a high-resolution investigation of *in vivo* progression of atherosclerosis and vulnerable plaque rupture. Using the Constantinides' model of atherothrombosis, we were able to image inflammation distribution *prior* to triggered plaque thrombosis. Because the CLIO-CyAm7 imaging agent has not been previously used in a large animal model, extensive *ex vivo* investigation was performed to better characterize the distribution of the imaging agent in rabbit atherosclerosis.

While human coronary plaque inflammation is clearly linked to plaque rupture and acute myocardial infarction, there is scant data regarding whether *in vivo* measures of plaque macrophages predict plaque rupture. Previous studies using PET and MRI in this model have indicated that macrophages and inflammation are likely to play an important predictive role in the development of plaque rupture. However, the relatively low resolution of these imaging modalities, compared to intravascular approaches, limits the ability to assess predictive value on a per-plaque basis. Therefore, intravascular NIRF imaging with CLIO-CyAm7 provides a clinically translatable approach to assess the role of inflammation in vulnerable plaques *in vivo* prior to plaque rupture. We hypothesized that more inflamed plaques, as measured by fluorescence signal from CLIO-CyAm7 both through *in vivo* 2D NIRF imaging and *ex vivo*

fluorescence imaging, will be more likely to rupture and develop thrombosis after pharmacological triggering.

METHODS

Animal Model of Atherothrombosis

We used an established rabbit model of aorta atheroma that reliably developed inflamed macrophage-rich lesions that later generated plaque rupture under triggering conditions**.(70-72, 75)** An overview of the triggered plaque rupture model is shown in Figure 1. New Zealand white rabbits (n=28, weight 3-4kg, Charles River Laboratories) at 3-4 months of age were fed a HCD (1% cholesterol, Research Diets, Inc., New Brunswick, NJ) to promote atheroma formation. At two weeks, a trained animal surgeon in the Jaffer Lab (Adam Mauskapf) performed balloon denudation of the aorta to cause endothelial injury and accelerate atheroma formation. For balloon injury, anesthesia was induced using injection of Ketamine (45mg/kg) and Xylazine (5.5mg/kg), and was continued using inhaled isoflurane (2% mixture). A 3F Fogarty catheter (Edwards Lifesciences, Irvine, CA) was advanced to the abdominal aorta via the femoral artery using a cut down of the femoral artery and fluoroscopic guidance. The balloon was inflated to tension and 3 pullbacks were performed over a 6 cm area distal to the renal arteries.

After balloon injury, rabbits continued on 1% HCD for six weeks, followed by four weeks of normal diet. Alternating diets along with balloon injury produced a variety of plaques, including inflamed, macrophage-rich and stable fibrous plaques. At 10 weeks after balloon injury, survival imaging was performed.(70-72) CLIO-CyAm7 (2.5 mg Fe/kg or 5.0mg Fe/kg) was injected intravenously twenty-four hours prior to *in vivo* imaging. CLIO-CyAm7 is a dextran coated cross-linked iron oxide core conjugated to a CyAm7 fluorophore. The agent was synthesized in the laboratory of our collaborator, Dr. Jason McCarthy (MGH Center for Systems Biology). Earlier studies determined that a 2.5mg/kg dosage 24 hours prior to imaging provided sufficient signal-to-noise ratio (SNR) and prevented toxicity to the rabbits. However, due to the broad spectrum of Evans Blue fluorescence there was some overlap with the near-infrared spectrum, so a higher dose of CLIO-CyAm7 (5.0mg/kg) was used in rabbits injected with Evans Blue to increase the CLIO-CyAm7 signal. Immediately following survival imaging, a subset of rabbits (n=6) was sacrificed for control microscopy of CLIO-CyAm7. In the remaining rabbits (n=22), pharmacological triggering was initiated by injection of Russell's Viper Venom (0.15mg/kg IP, Sigma Chemical Co, St Louis, MO) followed 30 minutes later by histamine (0.02mg/kg IV, Sigma Chemical Co). This triggering protocol was performed twice at a twenty-four hour

interval. Forty-eight hours after imaging, animals were reimaged using x-ray angiography and IVUS imaging to detect thrombus *in vivo*, as described below. Rabbits receiving 5.0mg Fe/kg CLIO-CyAm7 (n=7) were injected with Evans Blue (6mL 0.5%, Sigma Chemical Co) 30 minutes prior to sacrifice to measure permeability of atheroma.(48) All rabbits were then sacrificed and perfused with saline. All animal protocols were approved by the Massachusetts General Hospital Subcommittee on Research Animal Care.

Multimodal Arterial Imaging

At the time of survival imaging, rabbits were anesthetized as described previously and a 5F introducer was placed into the right carotid artery, followed by a 5F catheter advanced to the abdominal aorta. X-ray angiography with iodinated contrast was performed at this time (Varic, Siemens).

Intravascular Near Infrared Fluorescence Imaging

Imaging of the macrophage signal in atheroma was performed using a custom-built 2D intravascular NIRF imaging system that allows 360 degree imaging through blood.(62) A diagram of this system is included in Figure 2. A clinical-type intravascular catheter was placed percutaneously through the carotid artery into the rabbit aorta. A continuous wave near-infrared fiber-coupled laser (ex 750nm) was interfaced to the catheter. The optical fiber was encased in a polyethylene sheath to allow smooth rotation of the fiber. The laser light excited fluorochromes in the artery wall, and the emitted fluorescent light was filtered and transmitted back down the catheter to be captured. The wire was mechanically rotated and retracted to produce a 2D image of the vessel wall, which was visualized using MATLAB version 7.12.0 (2011, MathWorks, Natick, MA).(62, 63, 76, 77)

Four pullbacks from the iliac bifurcation to the renal arteries of approximately 90mm were performed, with two different placements of the lead wire. During *in vivo* NIRF imaging, x-ray fluoroscopy of the radiopaque tip was used to determine the exact location of the beginning and end points of each pullback to coregister *in vivo* NIRF with IVUS radiopaque markers and *ex vivo* fluorescence reflectance imaging (FRI).

NIRF Signal Analysis

Analysis of NIRF images was completed using MATLAB. Raw signal from the imaging system was converted into a two-dimensional matrix representing the length of the aorta and the rotational angles. The raw signal was filtered using a low pass filter and the background was

subtracted.

To analyze NIRF images, the filtered signal was averaged over 3mm segments along the length of the aorta (MATLAB). Using pre-trigger IVUS images, segments were characterized as either plaque or normal vessel based on neointimal thickening. Additionally, using post-trigger IVUS images and *ex vivo* histology, plaque segments were determined to be either non ruptured or ruptured, defined as attached luminal thrombus on IVUS or determined by *ex vivo* Carstairs' staining of red fibrin. Due to the distance dependent sensitivity of 2D NIRF imaging, the NIRF signal was excluded for any segments with an average vessel diameter greater than 5mm as measured on IVUS images.

Images were quantified using target-to-background ratio (TBR) and SNR analyses. TBR was defined as the signal from an area of plaque divided by the signal from a normal, uninjured segment of the aorta. SNR was defined as the signal measured *in vivo* divided by the standard deviation of the background noise, measured at each imaging session prior to insertion of the catheter into the body. The length of the aorta was divided into six 1.5cm segments, correlating with *ex vivo* imaging and histology for analysis. For each segment, the maximal TBR from each of the four 2D NIRF pullback images was calculated (MATLAB).

Intravascular Ultrasound Imaging

IVUS allows high resolution imaging of arterial structure and atherosclerotic plaques (plaque volume, remodeling index) during *in vivo* imaging. IVUS is routinely used in clinical coronary imaging. The 3.2 French IVUS catheter (40mHz 0.5mm/sec pullback Galaxy IVUS System, Boston Scientific, Natick, Massachusetts) was inserted into the carotid artery. Serial helical pullbacks from the iliac bifurcation to the renal artery produced a three-dimensional data set. Fluoroscopy was used before and after IVUS imaging for future co-registration with other imaging modalities. IVUS imaging was also performed at the time of sacrifice to visualize luminal thrombus after pharmacological triggering. Vessel diameter was calculated by averaging the diameter in two perpendicular planes

***Ex Vivo* Imaging**

Fluorescence Reflectance Imaging (FRI)

FRI imaging allows macroscopic imaging and quantification of fluorescence signals from CLIO-CyAm7 and autofluorescence along the entire length of the aorta. Resected vessels were

imaged using FRI (Kodak Carestream 4000 MMPro) with NIR filter set (Omega Optical, Brattleboro, Vermont): bandpass excitation: 716 to 756 nm, bandpass emission: 780 to 820 nm. A 16 second exposure time was used to image CLIO-CyAm7 and autofluorescence signals. Due to vessel shrinkage after resection of the artery, the vessel was elongated to the *in vivo* length determined by angiography. A segment of the renal artery, which has not been instrumented, was used as a normal control for TBR analysis. Additionally, a portion of the Kupffer-cell rich liver was imaged as a positive macrophage control for CLIO-CyAm7.

Histopathology

Resected vessels were systematically divided into 1.5 cm segments after elongation to *in vivo* length, marked with tissue marking ink, and embedded in optical cutting temperature compound (Sakura, Finetek, Torrance, CA). The aorta was cut in 6μm cryosections. Adjacent sections were stained using Carstair's stain to assess general morphology, collagen structure and to identify fibrin rich thrombi, RAM-11 macrophage specific immunofluorescence (IF), CD31 IF for endothelial cells, and α-smooth muscle actin (aSMA) IF for smooth muscle cells. For immunofluorescence, mouse anti-Rabbit RAM11 primary antibody (1:200 dilution, Dako), mouse anti-CD31 primary antibody (1:200 dilution, Abcam), and mouse anti-aSMA (1:100 dilution, Abcam) were incubated on adjacent sections with secondary goat anti-mouse Texas Red antibody (1:200 dilution, Abcam) for 45 minutes and then mounted with a coverslip. RAM11 IHC was also performed using mouse anti-Rabbit Ram11 primary antibody (1:500 dilution, Dako), then incubated with secondary anti-mouse Alkaline Phosphatase-conjugated antibody, stained using Vulcan fast red chromagen (Biocare medical) for 5 minutes, and counterstaining with hematoxylin.

Fluorescence microscopy

Fluorescence microscopy (FM) was performed using an epifluorescence microscope (Eclipse 90i, Nikon Instruments, Melville, New York). CLIO-CyAm7 was visualized on unstained sections and after IF staining with filters for NIRF (ex/em: 710/810nm, 500ms exposure). Evans blue and IF secondary antibodies (RAM11, CD31, and aSMA) were imaged using Texas Red filter (ex/em 590/620nm, 100ms exposure). Autofluorescence (ex/em 480/535nm; 500ms exposure) was measured during all fluorescence microscopy. Unstained CLIO-CyAm7 FM was acquired at 10x magnification. Immunofluorescence Images were acquired at 40x magnification. All FM analysis was done using ImageJ (National Institutes of Health, Bethesda, MD).

CLIO-CyAm7 distributions were analyzed in unstained, noncoverslipped sections of all rabbits at

0.5cm intervals along the aorta at 10x magnification. Thresholded images were used to define location of CLIO-CyAm7 as surface intima (superficial 100μm), deep intima (below 100μm, superficial to the internal elastic lamina), media (between the internal and external elastic lamina as seen on autofluorescence), and adventitia. A region of interest (ROI) for analysis included all tissue from the luminal edge of the vessel to 100um deep, in order to include all CLIO-CyAm7 signal from the superficial intimal layer without including any signal from the media or adventitia due to the surface predominance of *in vivo* NIRF imaging. Images were quantified by thresholding CLIO-CyAm7 signal at a constant level for all sections and calculating percent positive area. Each section was determined to be either plaque or normal vessel based on neointimal thickening and as rupture or non-rupture based on adjacent Carstair's staining identification of attached fibrin-rich thrombi. For analysis, the maximum value (% positive area) was chosen for each 1.5cm segment to correspond with NIRF analysis given the uncertainty of precise location of plaque rupture given ex vivo processing.

Statistical Analysis

All statistical analyses were completed using GraphPad Prism version 5.0c for Mac OSX (GraphPadSoftware, San Diego California USA, www.graphpad.com). For all 2D NIRF TBR and microscopy analyses between two groups, the nonparametric Mann-Whitney U test. Data is presented as mean ± standard deviation.

RESULTS

Rabbit Model of Atherothrombosis

Twenty-eight rabbits completed the 12-week alternating high cholesterol diet protocol. Six were sacrificed after *in vivo* imaging 24 hours after CLIO-CyAm7 injection, and seven were treated with Evans Blue to detect plaque permeability after triggered plaque thrombosis. Of the remaining fifteen rabbits completing the triggering protocol, 10 rabbits developed plaque thrombosis (67%). For analysis of both *in vivo* and *ex vivo* data, the length of each aorta was segmented into six 1.5 cm segments spanning from the bifurcation of the iliac arteries to the renal arteries.

The animal protocol used in this study produced a variety of plaque pathologies.(70) Aortic balloon denudation was initially performed by animal surgeon Adam Mauskapf on a section of the abdominal aorta between the iliac bifurcation and the renal arteries. This resulted in plaque formation in all rabbits with at least 1.5cm of control, uninjured aorta as measured by IVUS. To

confirm the presence of atheroma and categorize the different plaques, adjacent 6μm sections were stained with Carstairs' stain for morphology, collagen and fibrin.

In the areas of balloon injury a variety of plaque types developed in response to endothelial denudation and HCD. For example, a subset of plaques was fibrofatty with thick fibrous caps overlying a core of foam cell macrophages (Figure 3A). Additionally, a subset of inflamed, fatty plaques with very thin fibrous caps was present (Figure 3B). The diversity of plaques allowed a more comprehensive study of plaque vulnerability to pharmacologically triggered rupture.

Distribution of CLIO-CyAm7

As a novel agent, we investigated the cellular targeting of the CLIO-CyAm7 in atheroma. We utilized the fluorescence capability of the imaging agent by examining the distribution using immunofluorescence and fluorescence microscopy. CLIO-CyAm7 distribution along the length of the rabbit aorta was systematically and quantitatively assessed by calculating the percent positive area of CLIO-CyAm7 signal in a luminal 100μm band (ImageJ) in histological sections spaced every 0.5cm along the length of the atheroma. There was an increase in CLIO-CyAm7+ area in atheroma compared to control sections (Figure 4A, 1.73±1.9% and 0.13±0.28%, $p<0.0001$). CLIO-CyAm7 primarily accumulated in superficial, intimal macrophages with a small component in the media and adventitial layers. (Figure 4B)

Iron oxide nanoparticles have generally been thought to localize to macrophages; however, they have been found in multiple other cell types including endothelial cells and SMCs in atheroma.(59, 62) The major cell types in an atheromatous plaque capable of phagocytosing CLIO-CyAm7 include macrophages, smooth muscle cells and endothelial cells. These were assessed using immunofluorescence using RAM11, aSMA, and CD31 antibodies, respectively. CLIO-CyAm7 signal was found to correlate with each of these three cell types (Figure 5). However, CLIO-CyAm7 signal was only present within a subset of each cell type. For example, although RAM11+ macrophages may be identified throughout the intima, only a subset of superficial macrophages emanated CLIO-CyAm7 signal, suggesting that CLIO-CyAm7 cell uptake in part may be diffusion limited.

Mechanism of CLIO-CyAm7 Distribution

To better understand the mechanism of selective uptake of CLIO-CyAm7, two hypotheses were tested: CLIO-CyAm7 distribution is limited by permeability of the atheroma; and deeper penetration of CLIO-CyAm7 is dependent on the presence of local neovascularization. To

determine the permeability of the atheroma compared to CLIO-CyAm7 a subset of rabbits (n=7) were injected with Evans Blue 30min prior to sacrifice. Atheroma showed variable Evans Blue uptake which correlated well with the depth of penetration of subendothelial CLIO-CyAm7 (Figure 6). Additionally, Carstairs' imaging showed plaques with increased surface collagen (appearing blue with staining), indicating a thickened fibrous cap, in atheroma with decreased permeability and decreased CLIO-CyAm7 uptake. (Figure 6)

Neovascularization of the deep intima was identified from CD31+ endothelial cells lining the nascent blood vessels on immunofluorescence. CLIO-CyAm7 was detected in the deep intima, often at the intimal-medial border, only in plaques showing evidence of neovascularization. This subset of CLIO-CyAm7+ cells corresponded with RAM11+ macrophages, but not aSMA+ smooth muscle cells (Figure 7).

In Vivo Imaging of CLIO-CyAm7

We used multimodal imaging, including angiography, IVUS, and NIRF imaging, to obtain both the structural and inflammatory status prior to triggered plaque rupture.(62, 76, 77) All *in vivo* imaging data was co-registered using fluoroscopy and internal fiducials. IVUS readily identified areas of atheroma, as before. Additionally, both IVUS and angiography identified areas of aneurysmal enlargement in the aorta due to injury to the vessel. The average luminal diameter was 3.41±0.78mm, with a range of 1.93mm to 5.87mm. Aneurysmal segments limited the sensitivity of NIRF imaging due to attenuation of light by blood, therefore 2D NIRF data was excluded for segments with average diameters greater than 5mm. This is a reasonable exclusion threshold as most coronary arteries undergoing intravascular imaging have a diameter of 2.5-3.5mm. IVUS imaging was repeated after pharmacological triggering, prior to sacrifice, and macrothrombi were visible as luminal masses (Figure 8D,E,H).

To investigate the relationship of CLIO-demarcated atheroma cellular phagocytic activity *in vivo*, we used a 2D intravascular NIRF imaging system to measure CLIO-CyAm7 signal *in vivo,* prior to triggered plaque rupture.(62) Intravascular NIRF imaging had sufficient sensitivity to detect CLIO-CyAm7 signal through blood and identify areas of enhanced atheroma (Figure 8C). Atheroma had a significantly higher peak TBR compared to control, uninjured areas of the aorta (peak TBR 2.86±1.82 and 1.55±0.65, p=0.001, Figure 8I). This result shows the potential for *in vivo* NIRF imaging to identify macrophage-rich and phagocytically active plaques prior to plaque rupture and atherothrombosis. There was no significant difference in NIRF signal between

plaques showing thrombosis and no thrombosis. NIRF signal was verified ex vivo using FRI imaging and histology. (Figure 8F,G)

CLIO-CyAm7 Underlies Areas of Plaque Rupture

Of the 51 plaques analyzed, 21 showed evidence of attached thrombus on Carstairs' staining (41%). Thrombi were divided into two categories, macrothrombi (average area 3.96±3.97mm^2, n=13) and microthrombi (average area 0.19±0.13mm^2, n=8) based on size of thrombi on Carstairs' staining with a threshold of 0.5mm^2 due to the likelihood of visualization on IVUS.

In plaques with overlying thrombus, there was significantly higher percent CLIO-CyAm7+ area than atheroma without attached thrombus (2.1±1.7% and 1.5±1.9%, p=0.0446, Figure 9I). Microscopically, there was increased CLIO-CyAm7 accumulation directly underlying the thrombus and at the shoulder of plaques (Figure 9). IVUS images before and after plaque triggering showed that the thrombus formed as a result of triggering plaque rupture, after the injection of CLIO-CyAm7 (Figure 9G,H).

DISCUSSION

The pathogenesis and progression of atherosclerosis involves multiple biological processes dependent on interconnected pathologies. In this study, we translated a novel NIRF molecular imaging agent, termed CLIO-CyAm7, into a large animal model to track the role of inflammation and atheroma cell phagocytic activity in plaque rupture. We found that atheroma with greater CLIO-CyAm7 uptake correlated with an increased risk of plaque rupture for individual plaques. CLIO-CyAm7 identified inflamed macrophages and a subset of atheroma endothelial cells and smooth muscle cells linked to increased plaque permeability and increased vascularity.

Animal Model of Atherothrombosis

The atherothrombosis model used in this project had not been previously established within the Jaffer laboratory. Therefore, it was important to verify the diversity of plaques developed in this model and the success of triggered plaque thrombosis. The variety of plaques developed in these rabbits mimicked the diversity found in human disease, including stable fibrous plaques and thin cap, macrophage rich atheroma. The rate of plaque rupture (67%) was similar to the rates (60-70%) identified in the literature.(70-72, 74) This rate of rupture and diversity of plaques allowed a robust comparison of different plaque types.

Characterization of CLIO-CyAm7 Uptake

Although USPIOs have been used previously in the atherosclerosis literature, the new nanoparticle CLIO-CyAm7 had not been used in large animal models, like the rabbit.(52-54, 71, 78) CLIO-CyAm7 fluorescence microscopy demonstrated that this agent colocalized with a subset of plaque macrophages, endothelial cells and smooth muscle cells.

Previous studies of USPIO nanoparticles have shown various distributions in the rabbit model of atheroma. The majority of studies have shown a similar distribution of USPIO, both cross-linked and uncross-linked, uptake particularly in the subendothelial space with limited uptake along the internal elastic lamina.(54, 79-81) However, other studies have shown a deeper penetration of USPIOs with minimal subendothelial uptake.(82, 83) In our study, CLIO-CyAm7 showed a predilection for the subendothelial space with variable uptake along the internal elastic lamina and within the media. Additionally, CLIO-CyAm7 specifically accumulated at the shoulder regions of plaques, a site highly implicated in plaque rupture due to the mechanical stress in the region. Traditionally, iron oxide nanoparticles have been considered to be phagocytosed by macrophages, particularly due to the high uptake of iron oxide particles by macrophages in vitro.(57) However, our study and previous studies have shown that USPIOs are taken up heterogeneously by multiple cell types in macrophage-rich plaques in both rabbits and mice.(57, 59, 79)

Endothelial Cells

Endothelial cell dysfunction plays an important role from the first stage of atherosclerosis progression. CLIO-CyAm7 was found to colocalize with CD31+ endothelial cells on immunofluorescence. In the study by Cui et al, a similar CLIO NIRF particle called CLIO-VT680, was shown to localize to endothelium in a mouse model of arteriovenous fistula which similarly produced a phenotype of pathological endothelium and neointimal hyperplasia. In particular, they showed that uptake by endothelial cells was limited to abnormal endothelium as shown by VCAM-1 expression and increased permeability to Evans Blue.(59) Uptake of USPIOs by endothelial cells in the rabbit model of atherosclerosis has similarly been shown by electron microscopy.(80)

Smooth Muscle Cells

Uptake of CLIO-CyAm7 by aSMA+ smooth muscle cells has not been shown in the literature to play a major role in CLIO uptake. In fact, most IHC studies of rabbit atheroma using aSMA have failed to show a correlation with USPIO uptake.(63, 82, 83) The true extent of USPIO uptake by SMCs in the literature may be difficult to assess due to the various SMC phenotypes

thought to exist in atheroma. The typical contractile SMCs retain the SMC markers, such as alpha smooth muscle actin; however, these markers may be lost as SMCs undergo phenotypic change in the inflammatory mileu of the atheroma.

The role of SMCs is important for understanding plaque progression and rupture because production of extracellular matrix by synthetic SMCs is vital to maintaining a strong fibrous cap. Macrophages are known to induce apoptosis of SMCs, but there is increasing evidence of phenotype switching in atherosclerosis to an inflammatory SMC that produces adhesion molecules and cytokines that drive plaque progression. SMCs have been shown to express LDL and scavenger receptors that allow them to take up lipids similar to macrophages.(15, 17, 84) Due to the similarity in size between LDL and USPIOs, it is reasonable that these cells would be capable of phagocytosing CLIO-CyAm7. Interestingly in Ruehm et al, the clinically available uncross-linked USPIO Sinerem was found on electron microscopy to localize to cells with both macrophage and SMC characteristics, including the presence of both vacuoles and myosin.(79) The predilection of CLIO-CyAm7 for a subset of active smooth muscle cells with may provide a new tool for better understanding the interplay of different SMC phenotypes in atherosclerotic plaque progression and rupture.

Macrophages

Previous studies of USPIOs in the rabbit and mouse model have shown heterogenous uptake of USPIOs in macrophage rich plaques. Although the majority of macrophages in this model of atheroma are in the form of inactive foam cells, USPIO uptake does not occur in these cells, but rather occurs in smaller more active subendothelial macrophages.(80, 81, 83)

Further research into CLIO-CyAm7+ macrophages may contribute to the evolving field of plaque macrophage heterogeneity. Established categories of macrophage phenotypes include classically activated (M1) and alternatively activated (M2) macrophages.(12) Broadly speaking, M1 macrophages are proinflammatory and are associated with Th1 lymphocytes. M2 macrophages are associated with Th2 responses and are more commonly associated with regulating inflammatory responses and wound healing. Both cell types have been found in human and murine macrophages.(85) In the ApoE-/- mouse model of atherosclerosis, M2 macrophages dominated early lesions, with M1 macrophages dominating later. However, both macrophage types have been found to exist in plaques concurrently with different spatial distributions. Additionally, each macrophage subtype produces its own array of MMPs, contributing to destabilization of plaques. As the balance between different macrophage

phenotypes is better understood, the CLIO-CyAm7+ subset of cells may provide insight into macrophage diversity and subsequent plaque complications.

Mechanism of USPIO delivery

Distinct from the uptake of CLIO-CyAm7 on a cellular level, there is much controversy over the mechanism of delivery of USPIOs to atheroma. The prevailing theories are (1) recruitment of new USPIO+ monocytes to existing atheroma, (2) increased permeability due to endothelial dysfunction and (3) delivery of USPIO by the vaso vasorum. In our study, we investigated the role of permeability and vaso vasorum on CLIO-CyAm7 distribution.

Permeability of atheroma is due to endothelial dysfunction and fibrous cap thickness. CLIO-CyAm7 signal correlated with Evans blue-identified regions of increased permeability. Additionally, correlation with Carstairs imaging showed that areas of dense collagen deposition had limited CLIO-CyAm7 accumulation and Evans Blue penetration. Conversely, in thin cap fibroatheroma with minimal collagen, CLIO-CyAm7 penetrated deeper into the tissue and also exhibited increased Evans blue uptake.

During plaque progression, neovascularization occurs with growth of the vaso vasorum from the adventitia to the media and eventually into the deep intima. Increased angiogenesis may promote intraplaque hemorrhage and has been correlated with an increased risk of plaque rupture.(86) In the subset of rabbits with deep CLIO-CyAm7 signal, the agent accumulated along the internal elastic lamina in areas with evidence of CD31+ lined neovasculature. This indicates that neovascularization plays a role in delivery of CLIO-CyAm7 in a small subset of atherosclerotic plaques.

Multimodal In vivo imaging of CLIO-CyAm7 in Atherothrombosis

A reliable method of predicting plaque rupture will likely involve the integration of various parameters based on multimodal imaging. In this study, we utilized IVUS and intravascular NIRF imaging to provide both a structural and biological assessment of each plaque. IVUS imaging provided vital structural information about the location of atheroma in relation to 2D NIRF and the size of the lumen. Additionally, comparisons of pre- and post-trigger IVUS identified the location of macrothrombi in the lumen to provide an accurate correlation between 2D NIRF images and the location of plaque rupture, as well as *ex vivo* gross pathology, histology, and FRI. Unlike optical coherence tomography, IVUS does not have sufficient resolution to provide structural data about the thickness of the fibrous cap or location of

macrophages. Multimodality imaging can integrate inflammation status with already known risk factors for plaque disruption, like positive remodeling, fibrous cap thickness, and presence of lipids.

In vivo NIRF imaging detected a significant increase in CLIO-CyAm7 TBR in atheroma compared to the control, uninjured aorta. This indicates that 2D NIRF imaging is capable of detecting CLIO-CyAm7 fluorescence signal. Although FM showed a significant difference between ruptured and non-ruptured plaques, *in vivo* NIRF imaging did not have sufficient sensitivity to detect these changes with this limited sample size. The major obstacle to truly predictive imaging in this model is the propensity for aneurysm formation as a result of balloon injury. Human coronary arteries housing high-risk plaques are typically 2.5-3.5mm in diameter, and the 2D NIRF system has been developed to accurately assess fluorescence in vessels of this size.(62) However, in this rabbit model of atherosclerosis the diameter of the imaged arteries often exceeded 4mm, with the highest diameter of 5.88mm. This is beyond the distance detectable using the current 2D NIRF imaging system due to greater NIR light attenuation through blood. Contributing to this failure is the increased incidence of rupture in aneurysmal segments, limiting the *in vivo* imaging of vulnerable plaques.

CLIO-CyAm7 Signal is Increased in Plaques Susceptible to Thrombosis

The multiple mechanisms of CLIO-CyAm7 distribution incorporate the major drivers of plaque vulnerability: inflammation, endothelial dysfunction, reduced fibrous cap thickness and neovascularization. We found that plaques that developed thrombosis after pharmacologic triggering had a higher accumulation of CLIO-CyAm7 compared to atheroma without evidence of thrombosis. This supports the initial hypothesis that inflamed plaques with increased phagocytic capabilities, as measured by CLIO-CyAm7, may facilitate plaque disruption and subsequent thrombosis. In a previous study of this model using lower resolution ^{18}FDG-PET, it was found that rupture occurred in aortic segments with higher percent of RAM11+ macrophages. But specific local areas of increased macrophages and subsequent thrombosis were not demonstrated.(74) Although CLIO-CyAm7 does not appear to target a specific cell type or receptor, this agent identifies plaque cells with evidence of multiple factors contributing to plaque vulnerability.

This study is an important first step towards the development of intravascular molecular imaging in coronary arteries. The two major current methods of assessing arterial inflammation *in vivo* use MRI and PET imaging. USPIOs are ideal agents because a certain class of USPIOs,

ferumoxytol, is already FDA approved for clinical use. Therefore, iron oxide particles have been used to image inflammation in atherosclerosis using MRI.(52, 54, 78) By conjugating CLIO with a fluorophore to make CLIO-CyAm7, the precise distribution can be better mapped using high-resolution optical imaging, both *in vivo* and *ex vivo*. While PET is emerging as growing clinical tool for large artery atherosclerosis, the low resolution of PET limits its utility in the small, moving coronary arteries, and tracers such as FDG are limited by high background signal in the myocardium.(43) Intravascular NIRF imaging has the advantages of increased resolution and potential for translation to human coronary arteries.(40, 62, 76) Therefore, intravascular NIRF imaging of CLIO-CyAm7 is a promising translational tool for both understanding the role of inflammation in experimental plaque rupture and potential transition into clinical practice.

Limitations

Animal models are inherently limited in translatability to human disease progression. Although the atheroma developed using aortic denudation and HCD developed highly inflamed atheroma, some characteristics of human plaques, like large necrotic cores and cholesterol crystals, were not found in this rabbit model. Additionally, the model of atherothrombosis has limited applicability to spontaneous human plaque rupture. Although previous studies have reported identification of areas of discontinuous fibrous cap attached to thrombus, these specific rupture sites were not identified in this study. The two possible explanations for this difference are that this model shows micro-disruptions of the fibrous cap, or the sites of plaque rupture were simply not in the areas selected for histological analysis. Also, the aorta necessarily has different hemodynamic forces compared to human coronary arteries, like diastolic flow, which could affect atheroma rupture.

A major limitation to the histological analysis of CLIO-CyAm7 is that histology occurred 72 hours after CLIO-CyAm7 injection, and 48 hours after *in vivo* imaging, due to the time necessary for pharmacological triggering. This is the same limitation of all post-mortem analyses and histological studies and is the basis for continued development of *in vivo* imaging techniques that can map CLIO-CyAm7 distribution before pharmacological triggering. Due to the use 750nm wavelength of the CLIO-CyAm7 particle, we were unable to use commercial confocal microscopy systems to conclusively determine colocalization of the particle with various antibodies using IF. Additionally, the well-established primary antibodies for immunofluorescence in rabbits (RAM11, aSMA, and CD31) are raised in mice. Therefore, it was not possible to simultaneously stain for multiple antibodies on the same slide.

In vivo imaging using 2D intravascular NIRF imaging has some drawbacks that limited the ability to detect differences in signal between ruptured and non-ruptured plaques, which were identified in histology. One of the major limitations of *in vivo* 2D NIRF imaging is that the there is a distance dependent attenuation due to blood. In the typical rabbit aorta (diameter ~3mm) this does not pose a problem. However, in this model, there was often aneurysm formation, limiting the sensitivity of 2D NIRF imaging. Therefore, data was excluded if the diameter of a segment was greater than 5mm. However, even in included data points, this attenuation may have influenced the quantitative analysis of 2D NIRF signal. Using a combined 2D NIRF-OFDI system(40), structural information could be obtained simultaneously and allow for distance correction. However, the focused laser used in this combined system would further decrease signal from aneurysmal segments, a problem increased by the necessity of flushing the vessel with saline and the resulting expansion of the artery.

Future Directions

There are two major areas for future study with this project: improving *in vivo* NIRF imaging and understanding the biology of CLIO-CyAm7+ atheroma cells. To improve the *in vivo* 2D NIRF data, a larger number of rabbits are needed to increase the number of ruptured segments to study without aneurysm and increased sensitivity of the system. Increased sensitivity of the NIRF system could be obtained by either flushing with saline to remove attenuation by blood, or by utilizing an OFDI-NIRF combined system or newer IVUS-NIRF systems to be constructed. These systems allow post-imaging distance compensation for attenuation.

Understanding the biological implications of CLIO-CyAm7 uptake is also crucial. To further understand this aspect, further immunofluorescence and electron microscopy could be used. By using a different fluorochrome with excitation of <680nm, confocal microscopy would allow better colocalization of CLIO with immunofluorescence. *In vitro* cell culture of macrophages allows manipulation of levels of activation and analysis of the resultant changes in CLIO-CyAm7 uptake. Analysis of the expression of MMP9, MMP12, tissue factor, and other markers of macrophage activation can elucidate the activity of these macrophages to understand the importance of this subset of cells.

CONCLUSIONS

CLIO-CyAm7 is a novel magneto-optical NIRF molecular imaging agent that identified a unique subset of phagocytically active plaque macrophages, smooth muscle cells and endothelial cells in the rabbit model of atherothrombosis. Importantly, there was increased CLIO-CyAm7

accumulation in thrombosis-prone plaques on analysis by fluorescence microscopy, indicating increased inflammation in these high-risk plaques. *In vivo* intravascular NIRF imaging of CLIO-CyAm7 had sufficient sensitivity to detect this agent through blood; however, current limitations of the technology, model and sample size prevent the development of a true predictive model of plaque rupture based on *in vivo* imaging. This study lays a foundation for a deeper understanding of plaque cell heterogeneity as defined by CLIO-CyAm7 uptake and provides a promising future translational tool for high-resolution imaging of atheroma in human coronary arteries.

SUMMARY

Atherosclerosis is a systemic inflammatory disease that causes a thickening of the artery wall and contributes to major causes of death world wide, including coronary artery disease and stroke. Acute coronary events, like unstable angina, acute myocardial infarction, and sudden death, are the result of sudden luminal thrombosis from disruption of an atherosclerotic plaque. However, current imaging tools are unable to adequately predict the occurrence of these events. Inflammation is a major driving force behind the progression of atherosclerosis, providing an ideal target for molecular imaging. Therefore, we used a novel fluorescence imaging agent, CLIO-CyAm7, to image inflammation in a rabbit model of triggered atherothrombosis. We hypothesized that more inflamed plaques would be more susceptible to plaque disruption and thrombus formation.

We found that not only was CLIO-CyAm7 increased in atheroma compared to control segments, but also more importantly, plaques with thrombosis showed increased CLIO-CyAm7 accumulation compared to other areas of atheroma. CLIO-CyAm7 was found to localize to a subset of activated macrophages, smooth muscle cells and endothelial cells using immunofluorescence. Additionally, the mechanism of delivery of CLIO-CyAm7 to atheroma was further elucidated by showing increased permeability in plaques with increased subendothelial CLIO-CyAm7 and increase neovascularization in plaques with deep CLIO-CyAm7 signal. Intravascular *in vivo* near infrared fluorescence imaging allowed visualization of macrophage rich atheroma *in vivo* prior to plaque thrombosis. Nanoparticle enhanced fluorescence imaging may enhance our understanding of the role of inflammation in plaque thrombosis and provide a promising new method of detecting macrophage, smooth muscle cell and endothelial cell activity in human coronary arteries.

ACKNOWLEDGEMENTS

First, I would like to thank my thesis advisor, Dr. Farouc Jaffer, for all of his time, endless knowledge, and patience in helping me develop this project over the past four years. I would like to thank Adam Mauskapf the Jaffer lab animal surgeon and manager who performed all of the surgeries for this project and helped take care of the rabbits throughout. Dr. Jason McCarthy is our collaborator who developed CLIO-CyAm7 and provided us with the agent for this study.

This project was funded through Dr. Jaffer's NIH RO1 grant HL108229 and my funding was through the HST MD Research Assistantship and a one year American Heart Association Founder's Predoctoral Fellowship (2012-2013).

FIGURES

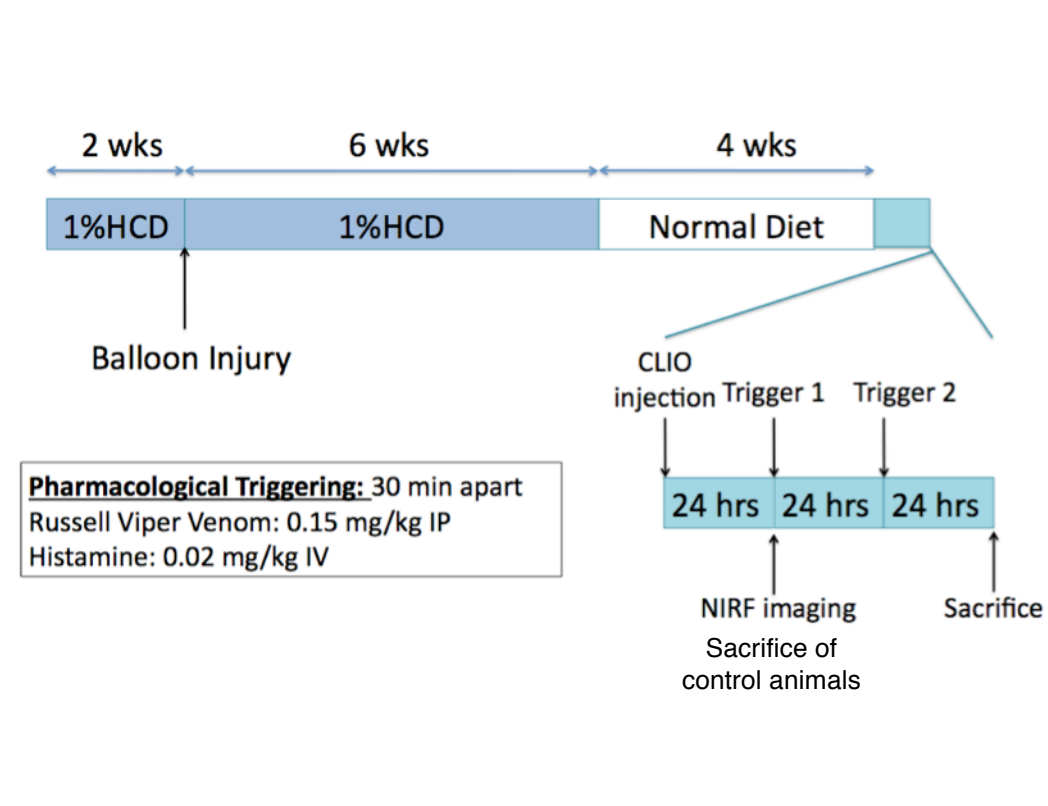

Figure 1: Schematic of the study design for the rabbit atherothrombosis model. Pharmacological triggering was performed using RVV (0.02mg/kg IV, Sigma Chemical Co) and histamine (0.02mg/kg IV, Sigma Chemical Co) 30 minutes apart. After sacrifice *ex vivo* imaging was performed.

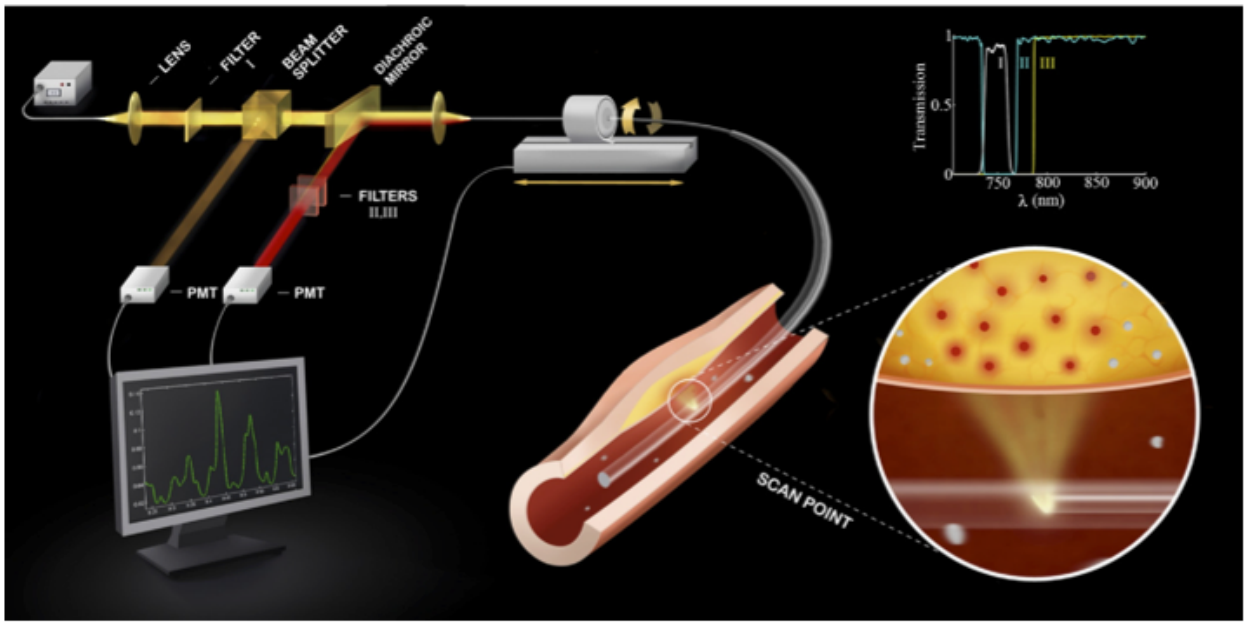

Figure 2: Diagram of 2D NIRF imaging system showing intravascular detection of a fluorescence agent in the vessel wall. Reproduced from Jaffer et al., *JACC* 2011.(62) A 750nm laser source is coupled to a catheter consists of an optical fiber within a polyethylene sheath to allow smooth pullback and rotation of the fiber within the sheath to generate a 2D signal. At the tip of the optical fiber, a prism reflects the laser light at a 90-degree angle towards the vessel wall. The resulting fluorescence light is then collected by the prism and reflected by a dichromatic mirror and beam splitter towards a photomultiplier tube (PMT) to be converted into a NIRF signal for analysis.

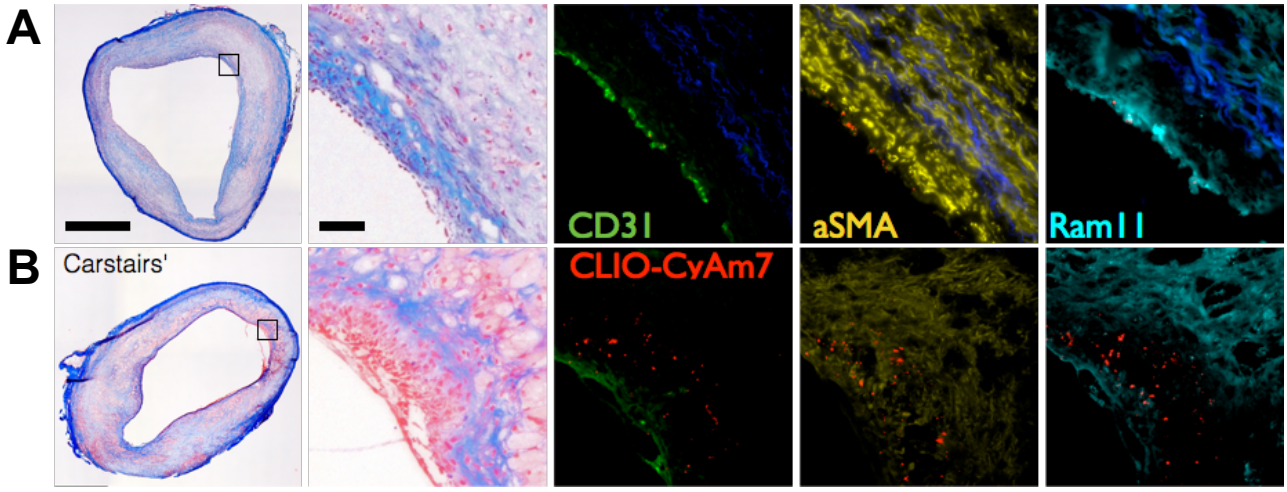

Figure 3: Various atheroma pathologies in a rabbit injected with CLIO-CyAm7 (2.5mg/kg). (A) Thick cap fibroatheroma with minimal superficial CLIO-CyAm7. CLIO-CyAm7 is limited to the endothelial layer and corresponds to CD31+ endothelial cells and superficial RAM11+ macrophages. (B) Thin cap atheroma with increased, surface CLIO-CyAm7 signal corresponding to subendothelial RAM11+ macrophages and aSMA+ smooth muscle cells. FM fusion images: CLIO-CyAm7-red, autofluorescence-blue, CD31-green, aSMA-yellow, RAM11-cyan. Carstairs': collagen – blue, fibrin – red. Column 1: 4x magnification, scale bar 1mm. Column 2-5: 40x magnification, scale bar 50μm.

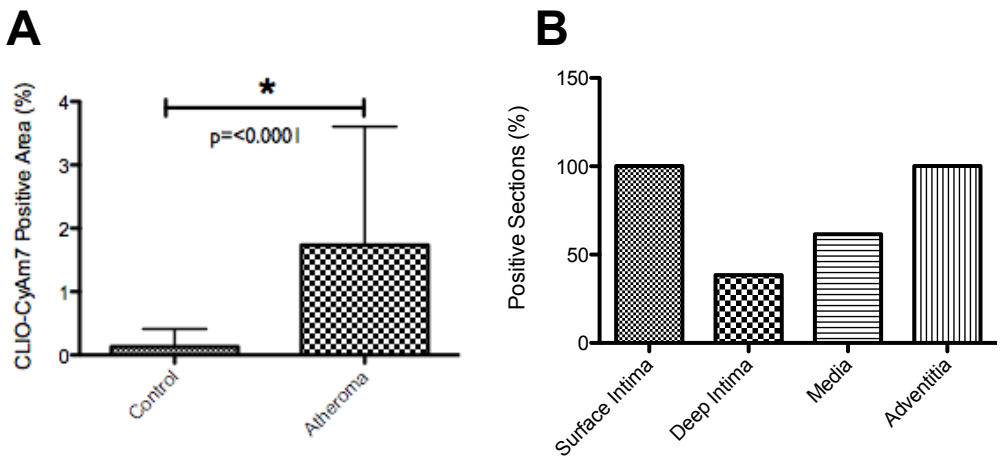

Figure 4: CLIO-CyAm7 accumulates within various layers of atheroma. (A) Fluorescence microscopy showed significantly higher percent positive area of CLIO-CyAm7 signal in areas of atheroma compared to normal, uninjured aorta segments (1.73±1.8% and 0.13±0.28%, respectively, p=0.003). (B) CLIO-CyAm7 localized in all plaques in both the surface intima, defined as the superficial 100μm segment, and the adventitia, beyond the external elastic lamina. CLIO-CyAm7 was variably identified in the deep intima, defined as starting 100μm from the lumen until the internal elastic lamina, and media, between the internal and external elastic lamina.

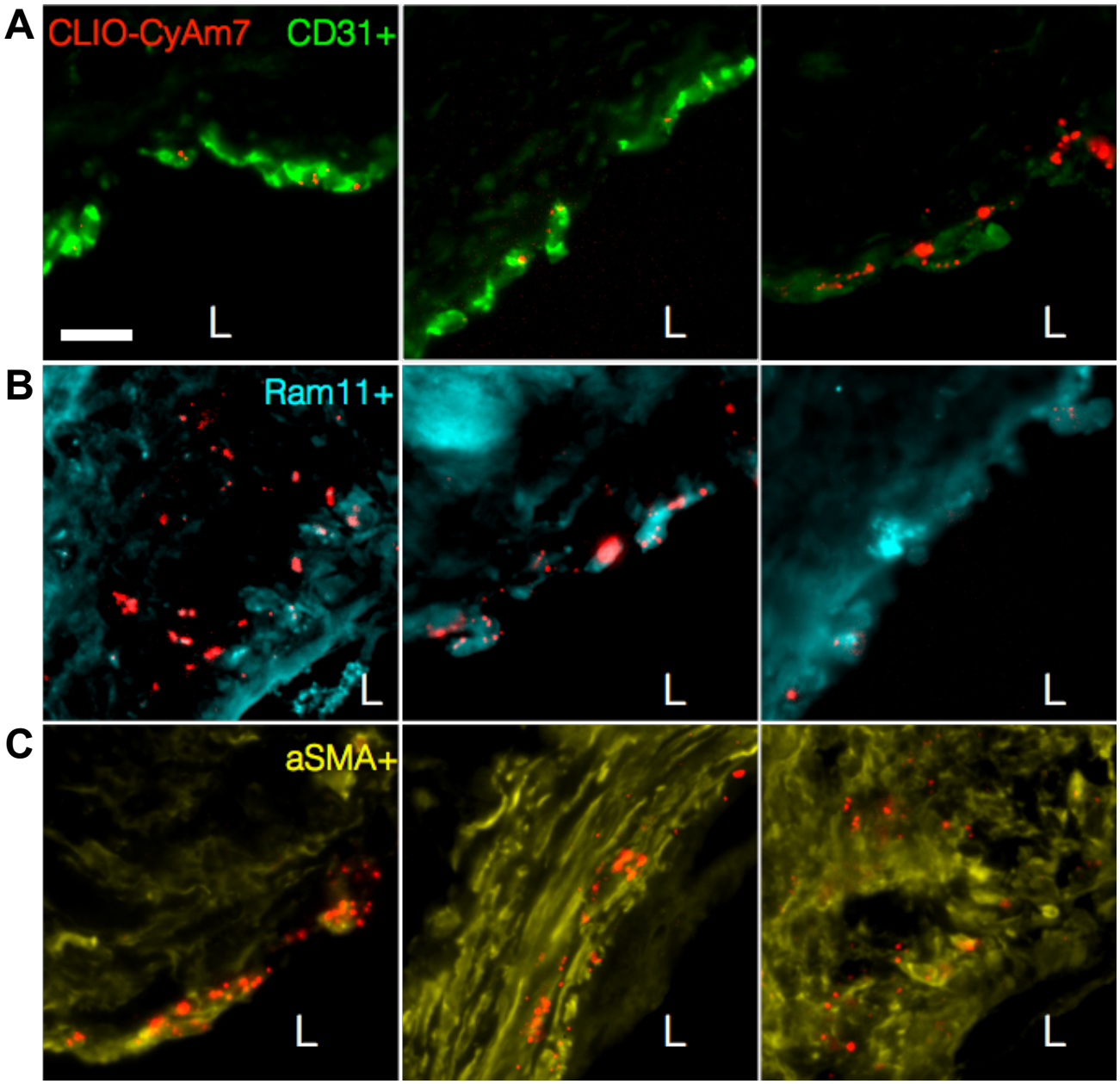

Figure 5: CLIO-CyAm7 uptake by endothelial cells, macrophages and smooth muscle cells. All images acquired at 40x magnification, L=vessel lumen. CLIO-CyAm7 = red, CD31 = Green, RAM11 = cyan, aSMA = yellow. (A) CLIO-CyAm7 signal correlated with surface CD31+ cells, indicating uptake of the agent by a subset of endothelial cells. (B) RAM11 positive macrophages showed uptake of CLIO-CyAm7 both on the plaque surface and in the subendothelial layer. (C) alpha-Smooth Muscle Actin (aSMA) + smooth muscle cells took up CLIO-CyAm7. Scale bar 25μm.

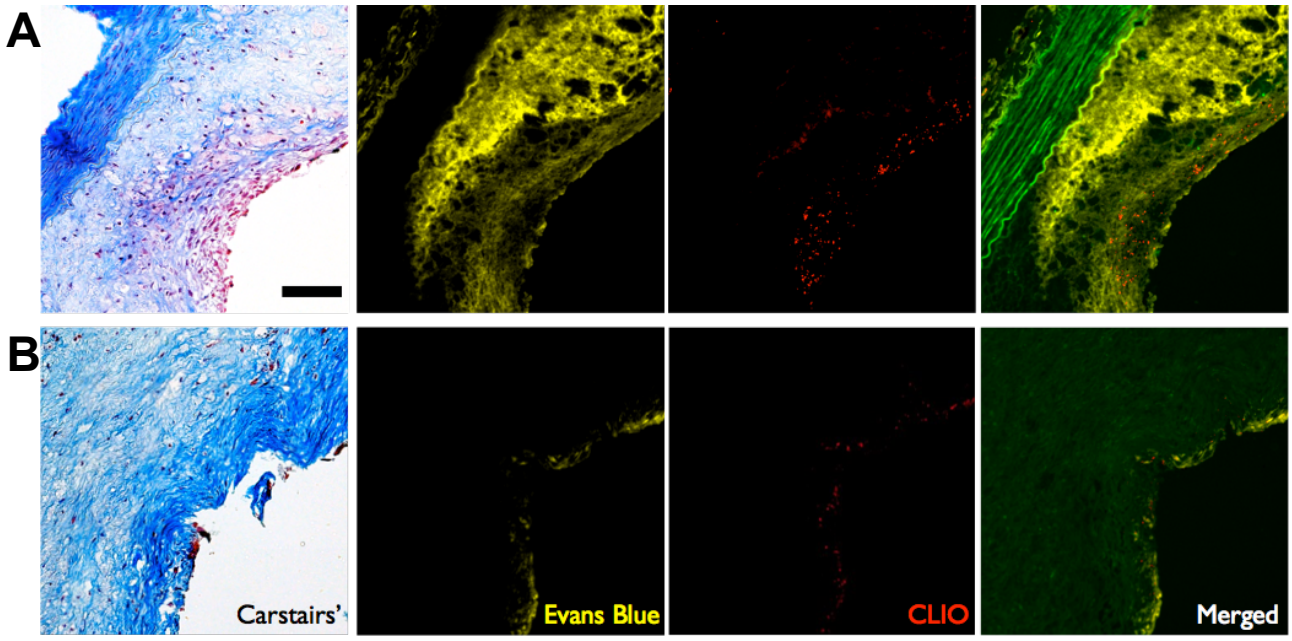

Figure 6: Plaque permeability assessed with Evans Blue in CLIO-CyAm7 injected rabbits. CLIO-CyAm7 = red, Evans Blue = Yellow, Autofluorescence = green. Different plaque types show varying *in vivo* Evans blue uptake. (A) Fatty atheroma with a thin fibrous cap on Carstairs showing shows extensive Evans blue uptake throughout the intima limited peripherally by the internal elastic membrane (seen on autofluorescence in green). CLIO-CyAm7 penetrates below the endothelial layer throughout the intima. (B) Atheroma with a thick fibrous layer, blue on Carstairs' staining with minimal, superficial Evans blue uptake and CLIO-CyAm7 signal limited to the endothelial layer. Scale bar 100μm.

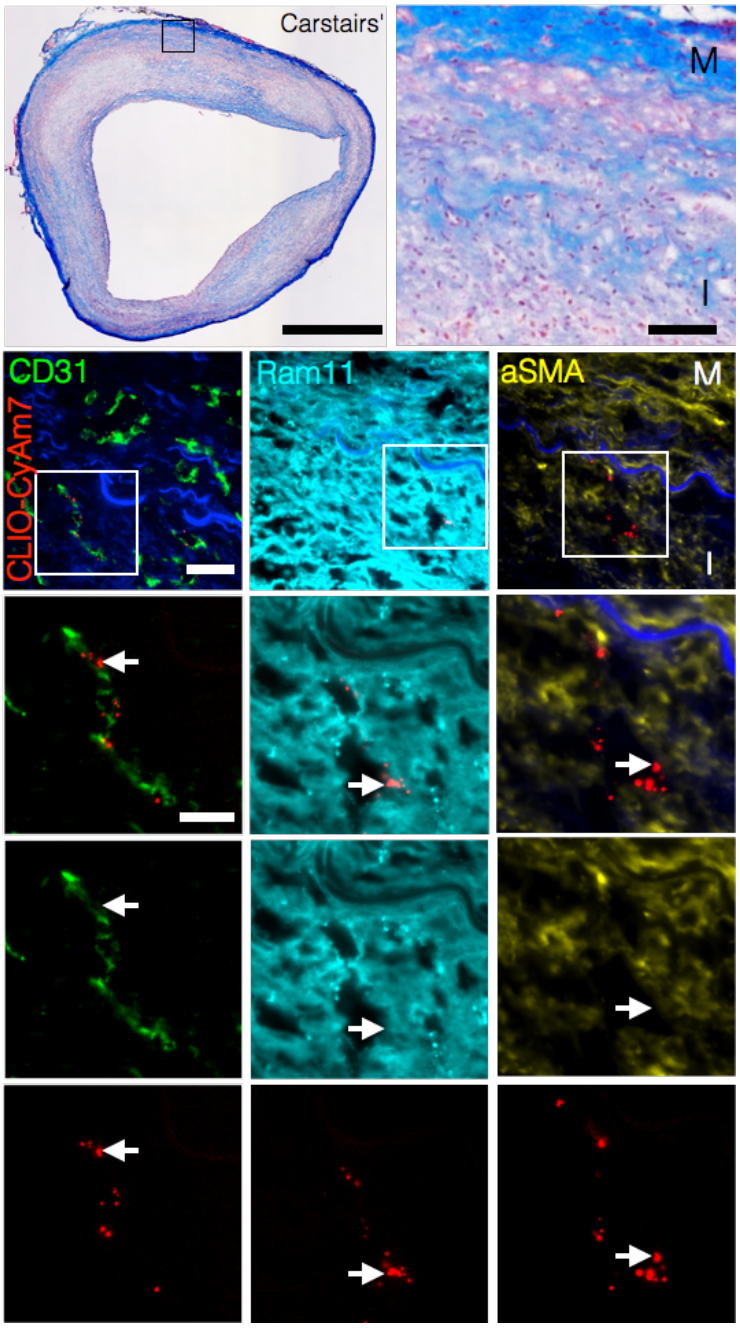

Figure 7: CLIO-CyAm7 distribution depends on vascularlity. CD31 IF showing increased vascularization within the deep intima. CLIO-CyAm7 signal occurs in the region of endothelial cell lined vessels, but also corresponds to RAM11 positive cells flanking the vessel. No correlation is seen with aSMA+ smooth muscle cells. All fluorescence microscopy images acquired at 40x magnification, L=vessel lumen. CLIO-CyAm7 = red, CD31 = Green, RAM11 = cyan, aSMA = yellow. Scale bars: Carstairs 4x = 1mm, Carstairs and IF 40x = 25 μm and 50 μm for inset.

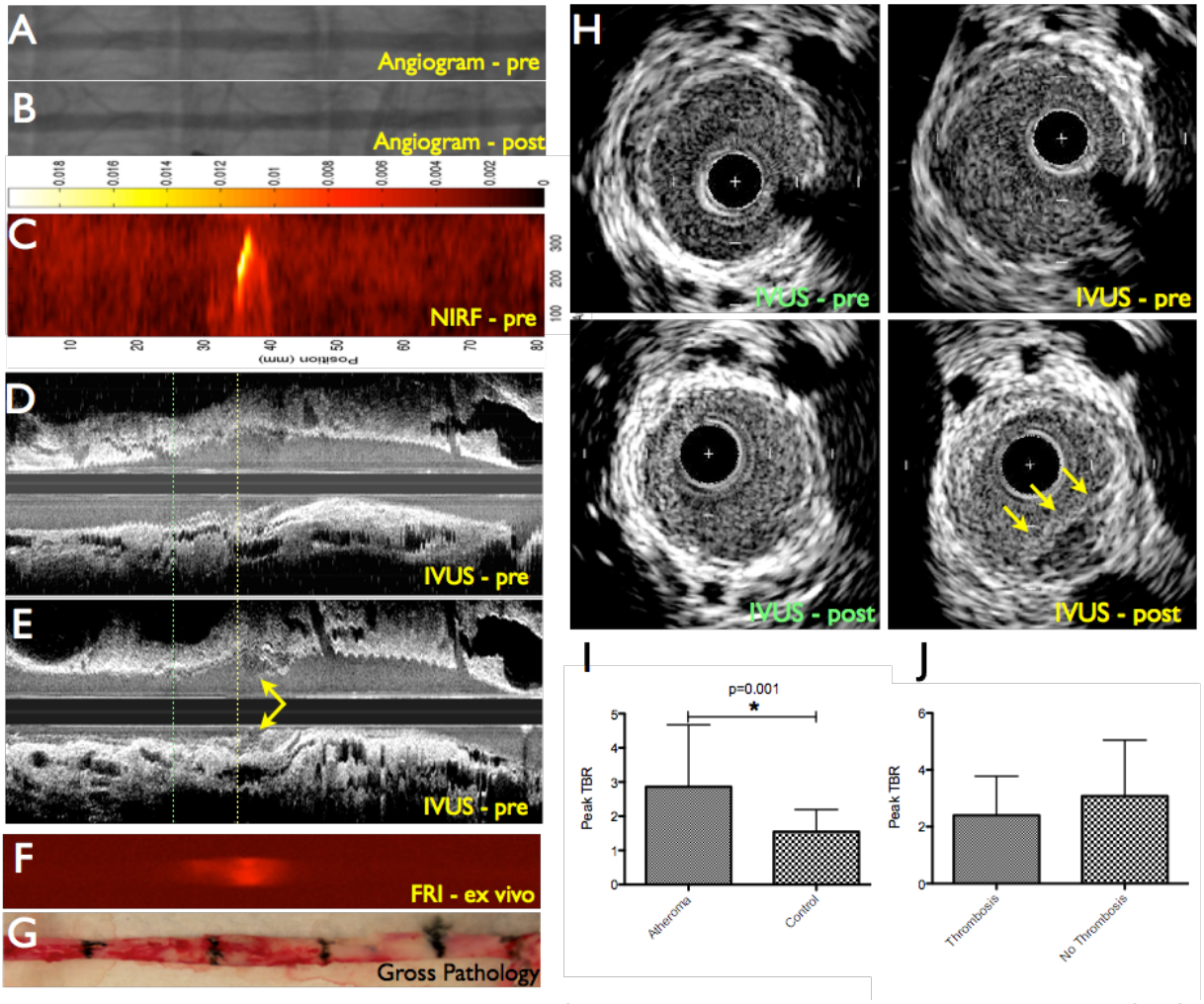

Figure 8: *In vivo* and *ex vivo* imaging data for an atherothrombosis rabbit injected with CLIO-CyAm7. (A,B) Pre- and post-trigger angiography. (C,D) Pre-trigger *in vivo* IVUS and NIRF imaging showing a focal region of high CLIO-CyAm7 signal intensity. (E) Post-trigger intravascular IVUS imaging showing triggered luminal thrombus (yellow arrows) corresponding to the region of increased NIRF signal intensity on pre-trigger NIRF imaging. (F) *Ex vivo* FRI of CLIO-CyAm7 verifying *in vivo* 2D NIRF imaging. (G) Gross pathology of resected aorta. Black markings are tissue marking ink delineating 1.5cm segments for histological analysis. (H) Cross-sectional IVUS images with columns 1 and 2 corresponding to the green and yellow dashed lines indicated on longitudinal IVUS imaging. Luminal thrombosis is seen on post-trigger cross-sectional area, indicated by yellow arrows. (I) *In vivo* 2D NIRF imaging showed significantly higher TBR in areas with atheroma, compared to uninjured segments of the aorta (peak TBR 2.86±1.82 and 1.55±0.65, p=0.001). (J) *In vivo* 2D NIRF showed no significant difference in the peak TBR between plaques with or without subsequent thrombosis (2.41±1.37 and 3.08±1.97, p=0.118).

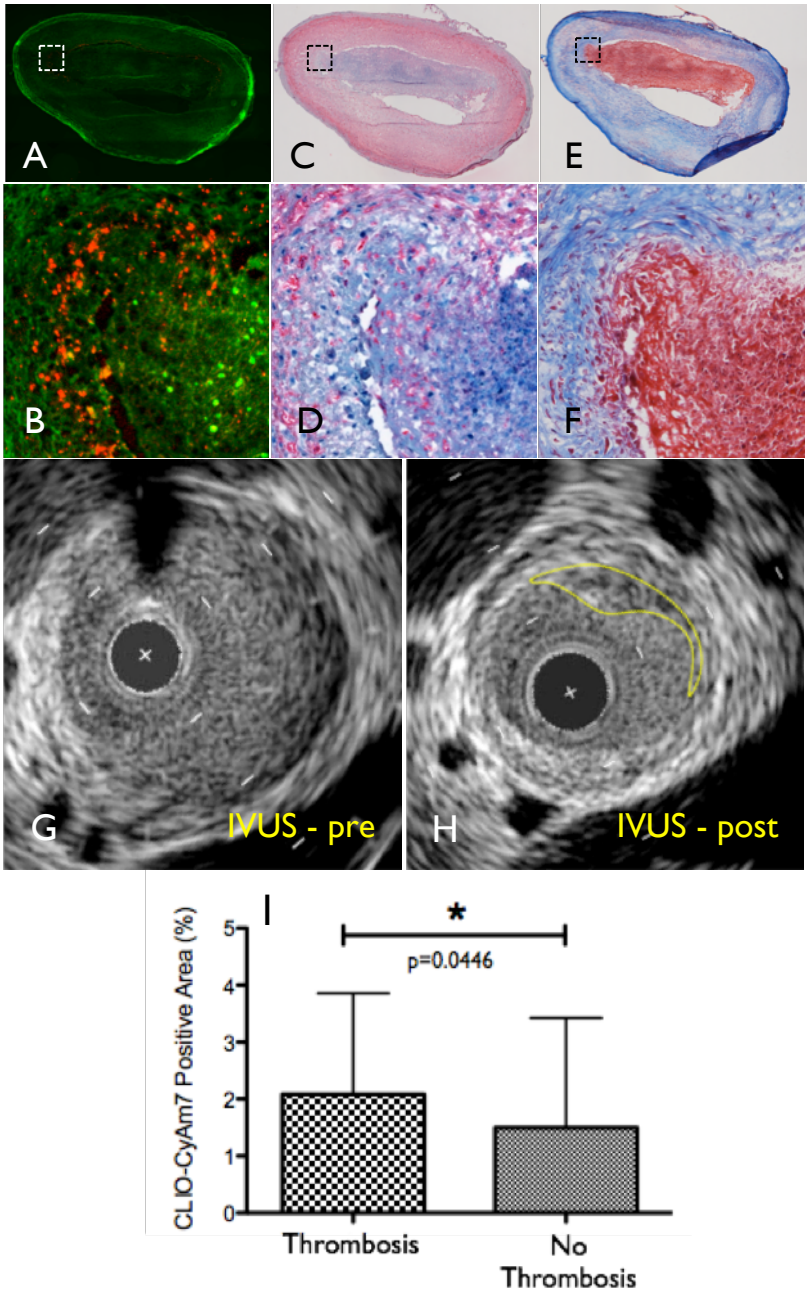

Figure 9: Histological and *in vivo* analysis of plaque rupture. (A,B) FM of plaque showing increased CLIO-CyAm7 (red) at the shoulder of the plaque and underlying areas of thrombus. FITC autofluorescence in green. (C,D) RAM11 immunohistochemistry for plaque macrophages, corresponding to CLIO-CyAm7 on FM. (E,F) Carstairs' staining with fibrin rich thrombus (red). (G,H) *In vivo* detection of thrombus using IVUS imaging in corresponding axial sections before and after thrombosis in yellow. Thrombus developed after triggering outlined in yellow. (I) (A) FM showed significantly higher percent positive area of CLIO-CyAm7 signal in areas of plaque thrombosis compared to areas without thrombosis (2.1±1.7% and 1.5±1.9%, p=0.0446).

REFERENCES

1. Stone GW, Maehara A, Lansky AJ, de Bruyne B, Cristea E, Mintz GS, Mehran R, McPherson J, Farhat N, Marso SP, Parise H, Templin B, White R, Zhang Z, Serruys PW, Investigators P. A prospective natural-history study of coronary atherosclerosis. N Engl J Med. 2011;364(3):226-35. doi: 10.1056/NEJMoa1002358. PubMed PMID: 21247313.
2. Arbab-Zadeh A, Nakano M, Virmani R, Fuster V. Acute coronary events. Circulation. 2012;125(9):1147-56. doi: 10.1161/CIRCULATIONAHA.111.047431. PubMed PMID: 22392862; PubMed Central PMCID: PMC3322378.
3. MacNeill BD, Lowe HC, Takano M, Fuster V, Jang IK. Intravascular modalities for detection of vulnerable plaque: current status. Arterioscler Thromb Vasc Biol. 2003;23(8):1333-42. doi: 10.1161/01.ATV.0000080948.08888.BF. PubMed PMID: 12805071.
4. Madjid M, Zarrabi A, Litovsky S, Willerson JT, Casscells W. Finding vulnerable atherosclerotic plaques: is it worth the effort? Arterioscler Thromb Vasc Biol. 2004;24(10):1775-82. doi: 10.1161/01.ATV.0000142373.72662.20. PubMed PMID: 15308556.
5. Chen IY, Wu JC. Cardiovascular molecular imaging: focus on clinical translation. Circulation. 2011;123(4):425-43. doi: 10.1161/CIRCULATIONAHA.109.916338. PubMed PMID: 21282520; PubMed Central PMCID: PMC3073678.
6. Jaffer FA, Libby P, Weissleder R. Molecular imaging of cardiovascular disease. Circulation. 2007;116(9):1052-61. doi: 10.1161/CIRCULATIONAHA.106.647164. PubMed PMID: 17724271.
7. Jaffer FA, Weissleder R. Molecular imaging in the clinical arena. JAMA. 2005;293(7):855-62. doi: 10.1001/jama.293.7.855. PubMed PMID: 15713776.
8. Sanz J, Fayad ZA. Imaging of atherosclerotic cardiovascular disease. Nature. 2008;451(7181):953-7. doi: 10.1038/nature06803. PubMed PMID: 18288186.
9. Go AS, Mozaffarian D, Roger VL, Benjamin EJ, Berry JD, Borden WB, Bravata DM, Dai S, Ford ES, Fox CS, Franco S, Fullerton HJ, Gillespie C, Hailpern SM, Heit JA, Howard VJ, Huffman MD, Kissela BM, Kittner SJ, Lackland DT, Lichtman JH, Lisabeth LD, Magid D, Marcus GM, Marelli A, Matchar DB, McGuire DK, Mohler ER, Moy CS, Mussolino ME, Nichol G, Paynter NP, Schreiner PJ, Sorlie PD, Stein J, Turan TN, Virani SS, Wong ND, Woo D, Turner MB, American Heart Association Statistics C, Stroke Statistics S. Heart disease and stroke statistics--2013 update: a report from the American Heart Association. Circulation. 2013;127(1):e6-e245. doi: 10.1161/CIR.0b013e31828124ad. PubMed PMID: 23239837.
10. Hansson GK. Inflammation, atherosclerosis, and coronary artery disease. N Engl J Med. 2005;352(16):1685-95. doi: 10.1056/NEJMra043430. PubMed PMID: 15843671.
11. Libby P, Ridker PM, Hansson GK. Progress and challenges in translating the biology of atherosclerosis. Nature. 2011;473(7347):317-25. doi: 10.1038/nature10146. PubMed PMID: 21593864.
12. Moore KJ, Tabas I. Macrophages in the pathogenesis of atherosclerosis. Cell. 2011;145(3):341-55. doi: 10.1016/j.cell.2011.04.005. PubMed PMID: 21529710; PubMed Central PMCID: PMC3111065.
13. Bentzon JF, Otsuka F, Virmani R, Falk E. Mechanisms of plaque formation and rupture. Circ Res. 2014;114(12):1852-66. doi: 10.1161/CIRCRESAHA.114.302721. PubMed PMID: 24902970.
14. Feil S, Fehrenbacher B, Lukowski R, Essmann F, Schulze-Osthoff K, Schaller M, Feil R. Transdifferentiation of vascular smooth muscle cells to macrophage-like cells during atherogenesis. Circ Res. 2014;115(7):662-7. doi: 10.1161/CIRCRESAHA.115.304634. PubMed PMID: 25070003.

15. Wall VZ, Bornfeldt KE. Arterial smooth muscle. Arterioscler Thromb Vasc Biol. 2014;34(10):2175-9. doi: 10.1161/ATVBAHA.114.304441. PubMed PMID: 25231633; PubMed Central PMCID: PMC4197844.
16. Orr AW, Hastings NE, Blackman BR, Wamhoff BR. Complex regulation and function of the inflammatory smooth muscle cell phenotype in atherosclerosis. Journal of vascular research. 2010;47(2):168-80. doi: 10.1159/000250095. PubMed PMID: 19851078; PubMed Central PMCID: PMC2842170.
17. Lim S, Park S. Role of vascular smooth muscle cell in the inflammation of atherosclerosis. BMB reports. 2014;47(1):1-7. PubMed PMID: 24388105; PubMed Central PMCID: PMC4163848.
18. Tabas I. The role of endoplasmic reticulum stress in the progression of atherosclerosis. Circ Res. 2010;107(7):839-50. doi: 10.1161/CIRCRESAHA.110.224766. PubMed PMID: 20884885; PubMed Central PMCID: PMC2951143.
19. Virmani R, Burke AP, Farb A, Kolodgie FD. Pathology of the vulnerable plaque. J Am Coll Cardiol. 2006;47(8 Suppl):C13-8. doi: 10.1016/j.jacc.2005.10.065. PubMed PMID: 16631505.
20. Boyle JJ, Weissberg PL, Bennett MR. Tumor necrosis factor-alpha promotes macrophage-induced vascular smooth muscle cell apoptosis by direct and autocrine mechanisms. Arteriosclerosis, thrombosis, and vascular biology. 2003;23(9):1553-8. doi: 10.1161/01.ATV.0000086961.44581.B7. PubMed PMID: 12869351.
21. Detrano R, Guerci AD, Carr JJ, Bild DE, Burke G, Folsom AR, Liu K, Shea S, Szklo M, Bluemke DA, O'Leary DH, Tracy R, Watson K, Wong ND, Kronmal RA. Coronary calcium as a predictor of coronary events in four racial or ethnic groups. N Engl J Med. 2008;358(13):1336-45. doi: 10.1056/NEJMoa072100. PubMed PMID: 18367736.
22. Hetterich H, Willner M, Fill S, Herzen J, Bamberg F, Hipp A, Schuller U, Adam-Neumair S, Wirth S, Reiser M, Pfeiffer F, Saam T. Phase-contrast CT: qualitative and quantitative evaluation of atherosclerotic carotid artery plaque. Radiology. 2014;271(3):870-8. doi: 10.1148/radiol.14131554. PubMed PMID: 24588675.
23. Shinohara M, Yamashita T, Tawa H, Takeda M, Sasaki N, Takaya T, Toh R, Takeuchi A, Ohigashi T, Shinohara K, Kawashima S, Yokoyama M, Hirata K, Momose A. Atherosclerotic plaque imaging using phase-contrast X-ray computed tomography. American journal of physiology Heart and circulatory physiology. 2008;294(2):H1094-100. doi: 10.1152/ajpheart.01149.2007. PubMed PMID: 18083896.
24. Takeda M, Yamashita T, Shinohara M, Sasaki N, Tawa H, Nakajima K, Momose A, Hirata K. Beneficial effect of anti-platelet therapies on atherosclerotic lesion formation assessed by phase-contrast X-ray CT imaging. Int J Cardiovasc Imaging. 2012;28(5):1181-91. doi: 10.1007/s10554-011-9910-6. PubMed PMID: 21688134.
25. Makowski MR, Botnar RM. MR imaging of the arterial vessel wall: molecular imaging from bench to bedside. Radiology. 2013;269(1):34-51. doi: 10.1148/radiol.13102336. PubMed PMID: 24062561.
26. Yuan C, Kerwin WS, Ferguson MS, Polissar N, Zhang S, Cai J, Hatsukami TS. Contrast-enhanced high resolution MRI for atherosclerotic carotid artery tissue characterization. Journal of magnetic resonance imaging : JMRI. 2002;15(1):62-7. PubMed PMID: 11793458.
27. Altaf N, Daniels L, Morgan PS, Auer D, MacSweeney ST, Moody AR, Gladman JR. Detection of intraplaque hemorrhage by magnetic resonance imaging in symptomatic patients with mild to moderate carotid stenosis predicts recurrent neurological events. Journal of vascular surgery. 2008;47(2):337-42. doi: 10.1016/j.jvs.2007.09.064. PubMed PMID: 18164171.
28. Botnar RM, Stuber M, Kissinger KV, Kim WY, Spuentrup E, Manning WJ. Noninvasive coronary vessel wall and plaque imaging with magnetic resonance imaging. Circulation. 2000;102(21):2582-7. PubMed PMID: 11085960.

29. Fayad ZA, Fuster V, Fallon JT, Jayasundera T, Worthley SG, Helft G, Aguinaldo JG, Badimon JJ, Sharma SK. Noninvasive in vivo human coronary artery lumen and wall imaging using black-blood magnetic resonance imaging. Circulation. 2000;102(5):506-10. PubMed PMID: 10920061.
30. Miao C, Chen S, Macedo R, Lai S, Liu K, Li D, Wasserman BA, Vogel-Claussen J, Lima JA, Bluemke DA. Positive remodeling of the coronary arteries detected by magnetic resonance imaging in an asymptomatic population: MESA (Multi-Ethnic Study of Atherosclerosis). J Am Coll Cardiol. 2009;53(18):1708-15. doi: 10.1016/j.jacc.2008.12.063. PubMed PMID: 19406347; PubMed Central PMCID: PMC2793325.
31. Gerretsen SC, Kooi ME, Kessels AG, Schalla S, Katoh M, van der Geest RJ, Manning WJ, Waltenberger J, van Engelshoven JM, Botnar RM, Leiner T. Visualization of coronary wall atherosclerosis in asymptomatic subjects and patients with coronary artery disease using magnetic resonance imaging. PloS one. 2010;5(9). doi: 10.1371/journal.pone.0012998. PubMed PMID: 20927368; PubMed Central PMCID: PMC2947500.
32. Oei ML, Ozgun M, Seifarth H, Bunck A, Fischbach R, Orwat S, Heindel W, Botnar R, Maintz D. T1-weighted MRI for the detection of coronary artery plaque haemorrhage. European radiology. 2010;20(12):2817-23. doi: 10.1007/s00330-010-1878-4. PubMed PMID: 20677007.
33. Hays AG, Hirsch GA, Kelle S, Gerstenblith G, Weiss RG, Stuber M. Noninvasive visualization of coronary artery endothelial function in healthy subjects and in patients with coronary artery disease. J Am Coll Cardiol. 2010;56(20):1657-65. doi: 10.1016/j.jacc.2010.06.036. PubMed PMID: 21050976.
34. Yeon SB, Sabir A, Clouse M, Martinezclark PO, Peters DC, Hauser TH, Gibson CM, Nezafat R, Maintz D, Manning WJ, Botnar RM. Delayed-enhancement cardiovascular magnetic resonance coronary artery wall imaging: comparison with multislice computed tomography and quantitative coronary angiography. J Am Coll Cardiol. 2007;50(5):441-7. doi: 10.1016/j.jacc.2007.03.052. PubMed PMID: 17662397.
35. Tardif JC, Lesage F, Harel F, Romeo P, Pressacco J. Imaging biomarkers in atherosclerosis trials. Circulation Cardiovascular imaging. 2011;4(3):319-33. doi: 10.1161/CIRCIMAGING.110.962001. PubMed PMID: 21586743.
36. Garcia-Garcia HM, Costa MA, Serruys PW. Imaging of coronary atherosclerosis: intravascular ultrasound. Eur Heart J. 2010;31(20):2456-69. doi: 10.1093/eurheartj/ehq280. PubMed PMID: 20823109.
37. Goldstein JA, Madden SP, Sum ST, Dixon SR, Madder RD, Muller JE. Assessment of Plaque Composition with Near-Infrared Spectroscopy. Current Cardiovascular Imaging Reports. 2011;4(4):298-308. doi: 10.1007/s12410-011-9095-3.
38. Komukai K, Kubo T, Kitabata H, Matsuo Y, Ozaki Y, Takarada S, Okumoto Y, Shiono Y, Orii M, Shimamura K, Ueno S, Yamano T, Tanimoto T, Ino Y, Yamaguchi T, Kumiko H, Tanaka A, Imanishi T, Akagi H, Akasaka T. Effect of atorvastatin therapy on fibrous cap thickness in coronary atherosclerotic plaque as assessed by optical coherence tomography: the EASY-FIT study. J Am Coll Cardiol. 2014;64(21):2207-17. doi: 10.1016/j.jacc.2014.08.045. PubMed PMID: 25456755.
39. Bezerra HG, Costa MA, Guagliumi G, Rollins AM, Simon DI. Intracoronary optical coherence tomography: a comprehensive review clinical and research applications. JACC Cardiovasc Interv. 2009;2(11):1035-46. doi: 10.1016/j.jcin.2009.06.019. PubMed PMID: 19926041; PubMed Central PMCID: PMC4113036.
40. Yoo H, Kim JW, Shishkov M, Namati E, Morse T, Shubochkin R, McCarthy JR, Ntziachristos V, Bouma BE, Jaffer FA, Tearney GJ. Intra-arterial catheter for simultaneous microstructural and molecular imaging in vivo. Nat Med.

2011;17(12):1680-4. doi: 10.1038/nm.2555. PubMed PMID: 22057345; PubMed Central PMCID: PMC3233646.
41. Kusters DH, Tegtmeier J, Schurgers LJ, Reutelingsperger CP. Molecular imaging to identify the vulnerable plaque--from basic research to clinical practice. Mol Imaging Biol. 2012;14(5):523-33. doi: 10.1007/s11307-012-0586-7. PubMed PMID: 22983911.
42. Libby P. Inflammation in atherosclerosis. Nature. 2002;420(6917):868-74. doi: 10.1038/nature01323. PubMed PMID: 12490960.
43. Buettner C, Rudd JH, Fayad ZA. Determinants of FDG uptake in atherosclerosis. JACC Cardiovasc Imaging. 2011;4(12):1302-4. doi: 10.1016/j.jcmg.2011.09.011. PubMed PMID: 22172787.
44. Satomi T, Ogawa M, Mori I, Ishino S, Kubo K, Magata Y, Nishimoto T. Comparison of contrast agents for atherosclerosis imaging using cultured macrophages: FDG versus ultrasmall superparamagnetic iron oxide. Journal of nuclear medicine : official publication, Society of Nuclear Medicine. 2013;54(6):999-1004. doi: 10.2967/jnumed.112.110551. PubMed PMID: 23670898.
45. Folco EJ, Sheikine Y, Rocha VZ, Christen T, Shvartz E, Sukhova GK, Di Carli MF, Libby P. Hypoxia but not inflammation augments glucose uptake in human macrophages: Implications for imaging atherosclerosis with 18fluorine-labeled 2-deoxy-D-glucose positron emission tomography. J Am Coll Cardiol. 2011;58(6):603-14. doi: 10.1016/j.jacc.2011.03.044. PubMed PMID: 21798423.
46. Tarkin JM, Joshi FR, Rudd JH. PET imaging of inflammation in atherosclerosis. Nature reviews Cardiology. 2014;11(8):443-57. doi: 10.1038/nrcardio.2014.80. PubMed PMID: 24913061.
47. Joshi NV, Vesey AT, Williams MC, Shah AS, Calvert PA, Craighead FH, Yeoh SE, Wallace W, Salter D, Fletcher AM, van Beek EJ, Flapan AD, Uren NG, Behan MW, Cruden NL, Mills NL, Fox KA, Rudd JH, Dweck MR, Newby DE. 18F-fluoride positron emission tomography for identification of ruptured and high-risk coronary atherosclerotic plaques: a prospective clinical trial. Lancet. 2014;383(9918):705-13. doi: 10.1016/S0140-6736(13)61754-7. PubMed PMID: 24224999.
48. Phinikaridou A, Andia ME, Protti A, Indermuehle A, Shah A, Smith A, Warley A, Botnar RM. Noninvasive magnetic resonance imaging evaluation of endothelial permeability in murine atherosclerosis using an albumin-binding contrast agent. Circulation. 2012;126(6):707-19. doi: 10.1161/CIRCULATIONAHA.112.092098. PubMed PMID: 22753191.
49. Vymazal J, Spuentrup E, Cardenas-Molina G, Wiethoff AJ, Hartmann MG, Caravan P, Parsons EC, Jr. Thrombus imaging with fibrin-specific gadolinium-based MR contrast agent EP-2104R: results of a phase II clinical study of feasibility. Invest Radiol. 2009;44(11):697-704. doi: 10.1097/RLI.0b013e3181b092a7. PubMed PMID: 19809344.
50. Overoye-Chan K, Koerner S, Looby RJ, Kolodziej AF, Zech SG, Deng Q, Chasse JM, McMurry TJ, Caravan P. EP-2104R: a fibrin-specific gadolinium-Based MRI contrast agent for detection of thrombus. Journal of the American Chemical Society. 2008;130(18):6025-39. doi: 10.1021/ja800834y. PubMed PMID: 18393503.
51. von Bary C, Makowski M, Preissel A, Keithahn A, Warley A, Spuentrup E, Buecker A, Lazewatsky J, Cesati R, Onthank D, Schickl N, Schachoff S, Hausleiter J, Schomig A, Schwaiger M, Robinson S, Botnar R. MRI of coronary wall remodeling in a swine model of coronary injury using an elastin-binding contrast agent. Circulation Cardiovascular imaging. 2011;4(2):147-55. doi: 10.1161/CIRCIMAGING.109.895607. PubMed PMID: 21378029.
52. Tang TY, Muller KH, Graves MJ, Li ZY, Walsh SR, Young V, Sadat U, Howarth SP, Gillard JH. Iron oxide particles for atheroma imaging. Arterioscler Thromb Vasc Biol. 2009;29(7):1001-8. doi: 10.1161/ATVBAHA.108.165514. PubMed PMID: 19229073.

53. Tang TY, Howarth SP, Miller SR, Graves MJ, Patterson AJ, JM UK-I, Li ZY, Walsh SR, Brown AP, Kirkpatrick PJ, Warburton EA, Hayes PD, Varty K, Boyle JR, Gaunt ME, Zalewski A, Gillard JH. The ATHEROMA (Atorvastatin Therapy: Effects on Reduction of Macrophage Activity) Study. Evaluation using ultrasmall superparamagnetic iron oxide-enhanced magnetic resonance imaging in carotid disease. J Am Coll Cardiol. 2009;53(22):2039-50. doi: 10.1016/j.jacc.2009.03.018. PubMed PMID: 19477353.
54. Morishige K, Kacher DF, Libby P, Josephson L, Ganz P, Weissleder R, Aikawa M. High-resolution magnetic resonance imaging enhanced with superparamagnetic nanoparticles measures macrophage burden in atherosclerosis. Circulation. 2010;122(17):1707-15. doi: 10.1161/CIRCULATIONAHA.109.891804. PubMed PMID: 20937980; PubMed Central PMCID: PMC3003265.
55. Weissleder R, Brian D. Ross PD, Rehemtulla A, Gambhir SS. Molecular Imaging, Principles and Practice: People's Medical Publishing House--USA; 2010.
56. Nahrendorf M, Jaffer FA, Kelly KA, Sosnovik DE, Aikawa E, Libby P, Weissleder R. Noninvasive vascular cell adhesion molecule-1 imaging identifies inflammatory activation of cells in atherosclerosis. Circulation. 2006;114(14):1504-11. doi: 10.1161/CIRCULATIONAHA.106.646380. PubMed PMID: 17000904.
57. Jaffer FA, Nahrendorf M, Sosnovik D, Kelly KA, Aikawa E, Weissleder R. Cellular Imaging of Inflainination in Atherosclerosis Using Magnetofluorescent Nanomaterials. Molecular Imaging. 2006;4:85-92.
58. Nahrendorf M, Zhang H, Hembrador S, Panizzi P, Sosnovik DE, Aikawa E, Libby P, Swirski FK, Weissleder R. Nanoparticle PET-CT imaging of macrophages in inflammatory atherosclerosis. Circulation. 2008;117(3):379-87. doi: 10.1161/CIRCULATIONAHA.107.741181. PubMed PMID: 18158358; PubMed Central PMCID: PMC2663426.
59. Cui J, Kessinger CW, McCarthy JR, Sosnovik DE, Libby P, Thadhani RI, Jaffer FA. In vivo nanoparticle assessment of pathological endothelium predicts the development of inflow stenosis in murine arteriovenous fistula. Arterioscler Thromb Vasc Biol. 2015;35(1):189-96. doi: 10.1161/ATVBAHA.114.304483. PubMed PMID: 25395614; PubMed Central PMCID: PMC4270948.
60. Leuschner F, Nahrendorf M. Molecular imaging of coronary atherosclerosis and myocardial infarction: considerations for the bench and perspectives for the clinic. Circ Res. 2011;108(5):593-606. doi: 10.1161/CIRCRESAHA.110.232678. PubMed PMID: 21372291; PubMed Central PMCID: PMC3397211.
61. Chen J, Tung CH, Mahmood U, Ntziachristos V, Gyurko R, Fishman MC, Huang PL, Weissleder R. In vivo imaging of proteolytic activity in atherosclerosis. Circulation. 2002;105(23):2766-71. PubMed PMID: 12057992.
62. Jaffer FA, Calfon MA, Rosenthal A, Mallas G, Razansky RN, Mauskapf A, Weissleder R, Libby P, Ntziachristos V. Two-dimensional intravascular near-infrared fluorescence molecular imaging of inflammation in atherosclerosis and stent-induced vascular injury. J Am Coll Cardiol. 2011;57(25):2516-26. doi: 10.1016/j.jacc.2011.02.036. PubMed PMID: 21679853; PubMed Central PMCID: PMC3123768.
63. Jaffer FA, Vinegoni C, John MC, Aikawa E, Gold HK, Finn AV, Ntziachristos V, Libby P, Weissleder R. Real-time catheter molecular sensing of inflammation in proteolytically active atherosclerosis. Circulation. 2008;118(18):1802-9. doi: 10.1161/CIRCULATIONAHA.108.785881. PubMed PMID: 18852366; PubMed Central PMCID: PMC2729441.
64. Ni M, Chen WQ, Zhang Y. Animal models and potential mechanisms of plaque destabilisation and disruption. Heart. 2011:1-7.
65. Watanabe Y. Serial inbreeding of rabbits with hereditary hyperlipidemia (WHHL-rabbit). Atherosclerosis. 1980;36(2):261-8. PubMed PMID: 7406953.

66. Kurz KD, Main BW, Sandusky GE. Rat model of arterial thrombosis induced by ferric chloride. Thrombosis research. 1990;60(4):269-80. PubMed PMID: 2087688.
67. Matsuno H, Uematsu T, Nagashima S, Nakashima M. Photochemically induced thrombosis model in rat femoral artery and evaluation of effects of heparin and tissue-type plasminogen activator with use of this model. Journal of pharmacological methods. 1991;25(4):303-17. PubMed PMID: 1909407.
68. Yamashita A, Asada Y. A rabbit model of thrombosis on atherosclerotic lesions. J Biomed Biotechnol. 2011;2011:424929. doi: 10.1155/2011/424929. PubMed PMID: 21253503; PubMed Central PMCID: PMC3021877.
69. Constantinides P, Chakravarti RN. Rabbit arterial thrombosis production by systemic procedures. Arch Pathol. 1961;72:197-208. PubMed PMID: 13695142.
70. Phinikaridou A, Hallock KJ, Qiao Y, Hamilton JA. A robust rabbit model of human atherosclerosis and atherothrombosis. J Lipid Res. 2009;50(5):787-97. doi: 10.1194/jlr.M800460-JLR200. PubMed PMID: 19141434; PubMed Central PMCID: PMC2666165.
71. Phinikaridou A, Ruberg FL, Hallock KJ, Qiao Y, Hua N, Viereck J, Hamilton JA. In vivo detection of vulnerable atherosclerotic plaque by MRI in a rabbit model. Circulation Cardiovascular imaging. 2010;3(3):323-32. doi: 10.1161/CIRCIMAGING.109.918524. PubMed PMID: 20194634.
72. Phinikaridou A, Hua N, Pham T, Hamilton JA. Regions of low endothelial shear stress colocalize with positive vascular remodeling and atherosclerotic plaque disruption: an in vivo magnetic resonance imaging study. Circulation Cardiovascular imaging. 2013;6(2):302-10. doi: 10.1161/CIRCIMAGING.112.000176. PubMed PMID: 23357244.
73. Hur J, Kim YJ, Shim HS, Lee HJ, Nam JE, Choe KO, Choi BW. Assessment of atherosclerotic plaques in a rabbit model by delayed-phase contrast-enhanced CT angiography: comparison with histopathology. Int J Cardiovasc Imaging. 2012;28(2):353-63. doi: 10.1007/s10554-011-9801-x. PubMed PMID: 21279690.
74. Aziz K, Berger K, Claycombe K, Huang R, Patel R, Abela GS. Noninvasive detection and localization of vulnerable plaque and arterial thrombosis with computed tomography angiography/positron emission tomography. Circulation. 2008;117(16):2061-70. doi: 10.1161/CIRCULATIONAHA.106.652313. PubMed PMID: 18391115.
75. Johnstone MT, Botnar RM, Perez AS, Stewart R, Quist WC, Hamilton JA, Manning WJ. In vivo magnetic resonance imaging of experimental thrombosis in a rabbit model. Arterioscler Thromb Vasc Biol. 2001;21(9):1556-60. doi: 10.1161/hq0901.094242. PubMed PMID: 11557688; PubMed Central PMCID: PMC2909772.
76. Razansky RN, Rosenthal A, Mallas G, Razansky D, Jaffer FA, Ntziachristos V. Near-infrared fluorescence catheter system for two-dimensional intravascular imaging in vivo. Opt Express. 2010;18(11):11372-81. doi: 10.1364/OE.18.011372. PubMed PMID: 20588998.
77. Zhu B, Jaffer FA, Ntziachristos V, Weissleder R. Development of a near infrared fluorescence catheter: operating characteristics and feasibility for atherosclerotic plaque detection. Journal of Physics D: Applied Physics. 2005;38(15):2701-7. doi: 10.1088/0022-3727/38/15/024.
78. Tang TY, Patterson AJ, Miller SR, Graves MJ, Howarth SP, JM UK-I, Li ZY, Sadat U, Young VE, Walsh SR, Boyle JR, Gaunt ME, Gillard JH. Temporal dependence of in vivo USPIO-enhanced MRI signal changes in human carotid atheromatous plaques. Neuroradiology. 2009;51(7):457-65. doi: 10.1007/s00234-009-0523-x. PubMed PMID: 19300987.
79. Ruehm SG, Corot C, Vogt P, Kolb S, Debatin JF. Magnetic resonance imaging of atherosclerotic plaque with ultrasmall superparamagnetic particles of iron oxide in hyperlipidemic rabbits. Circulation. 2001;103(3):415-22. PubMed PMID: 11157694.

80. Schmitz SA, Coupland SE, Gust R, Winterhalter S, Wagner S, Kriesse M, Seamler W, Wolf K-J. Superparamagnetic Iron Oxide-Enhanced MRI of Atherosclerotic Plaques in Watanabe Hereditable Hyperlipidemic Rabbits. [Article]. 2000 [updated Aug 01; cited 35]. 460-71].
81. Litovsky S, Madjid M, Zarrabi A, Casscells SW, Willerson JT, Naghavi M. Superparamagnetic iron oxide-based method for quantifying recruitment of monocytes to mouse atherosclerotic lesions in vivo: enhancement by tissue necrosis factor-alpha, interleukin-1beta, and interferon-gamma. Circulation. 2003;107(11):1545-9. PubMed PMID: 12654614.
82. Hyafil F, Laissy JP, Mazighi M, Tchetche D, Louedec L, Adle-Biassette H, Chillon S, Henin D, Jacob MP, Letourneur D, Feldman LJ. Ferumoxtran-10-enhanced MRI of the hypercholesterolemic rabbit aorta: relationship between signal loss and macrophage infiltration. Arterioscler Thromb Vasc Biol. 2006;26(1):176-81. doi: 10.1161/01.ATV.0000194098.82677.57. PubMed PMID: 16269663.
83. Yancy AD, Olzinski AR, Hu TC, Lenhard SC, Aravindhan K, Gruver SM, Jacobs PM, Willette RN, Jucker BM. Differential uptake of ferumoxtran-10 and ferumoxytol, ultrasmall superparamagnetic iron oxide contrast agents in rabbit: critical determinants of atherosclerotic plaque labeling. Journal of magnetic resonance imaging : JMRI. 2005;21(4):432-42. doi: 10.1002/jmri.20283. PubMed PMID: 15779033.
84. Doran AC, Meller N, McNamara CA. Role of smooth muscle cells in the initiation and early progression of atherosclerosis. Arterioscler Thromb Vasc Biol. 2008;28(5):812-9. doi: 10.1161/ATVBAHA.107.159327. PubMed PMID: 18276911; PubMed Central PMCID: PMC2734458.
85. Shalhoub J, Falck-Hansen MA, Davies AH, Monaco C. Innate immunity and monocyte-macrophage activation in atherosclerosis. J Inflamm (Lond). 2011;8(1):9. doi: 10.1186/1476-9255-8-9. PubMed PMID: 21526997; PubMed Central PMCID: PMC3094203.
86. Sadat U, Jaffer FA, van Zandvoort MA, Nicholls SJ, Ribatti D, Gillard JH. Inflammation and neovascularization intertwined in atherosclerosis: imaging of structural and molecular imaging targets. Circulation. 2014;130(9):786-94. doi: 10.1161/CIRCULATIONAHA.114.010369. PubMed PMID: 25156914; PubMed Central PMCID: PMC4212981.